

Flow Diagnostics and the Acoustic Behavior of a Fan-and-Coil Assembly

S. E. Zeller, R. L. Weaver, J. C. Dutton,
A. M. Jacobi, and S. Balachandar

ACRC TR-164

April 2000

For additional information:

Air Conditioning and Refrigeration Center
University of Illinois
Mechanical & Industrial Engineering Dept.
1206 West Green Street
Urbana, IL 61801

(217) 333-3115

*Prepared as part of ACRC Project 84
Flow Diagnostics and the Acoustic
Behavior of a Fan-and-Coil Assembly
J. C. Dutton, R. L. Weaver, A. M. Jacobi
and S. Balachandar, Principal Investigators*

The Air Conditioning and Refrigeration Center was founded in 1988 with a grant from the estate of Richard W. Kritzer, the founder of Peerless of America Inc. A State of Illinois Technology Challenge Grant helped build the laboratory facilities. The ACRC receives continuing support from the Richard W. Kritzer Endowment and the National Science Foundation. The following organizations have also become sponsors of the Center.

Amana Refrigeration, Inc.
Arçelik A. S.
Brazeway, Inc.
Carrier Corporation
Copeland Corporation
DaimlerChrysler Corporation
Delphi Harrison Thermal Systems
Frigidaire Company
General Electric Company
General Motors Corporation
Hill PHOENIX
Honeywell, Inc.
Husmann Corporation
Hydro Aluminum Adrian, Inc.
Indiana Tube Corporation
Invensys Climate Controls
Lennox International, Inc.
Modine Manufacturing Co.
Parker Hannifin Corporation
Peerless of America, Inc.
The Trane Company
Thermo King Corporation
Visteon Automotive Systems
Whirlpool Corporation
Wolverine Tube, Inc.
York International, Inc.

For additional information:

*Air Conditioning & Refrigeration Center
Mechanical & Industrial Engineering Dept.
University of Illinois
1206 West Green Street
Urbana IL 61801*

217 333 3115

ABSTRACT

Project 84 concentrated on understanding the noise generating mechanisms of axial-flow fans with the intent of proposing methods of component design and system assembly by which noise generation is reduced or minimized. The project focused on the fan-coil unit typical to room air conditioners and many split-system applications.

This report presents the accomplishments of the project, including the design, construction, and qualification of an anechoic chamber, the acquisition of acoustic, flow, and pressure data within a fan-coil unit over a typical operating range, and the development of an understanding of the flow-structure interactions responsible for noise generation in the fan-coil unit.

This report focuses on the investigation of a method for measuring the dynamic axial force generated by a fan operating in a steady but spatially non-uniform flow field. Several variations of a measurement system that uses a cantilever beam were tested. Experimental results indicated, in all designs, that the measurement system introduced additional sources of axial motion, occurring at the frequencies of interest and at amplitudes much larger than the one to be measured. Recommendations for future work are given.

CONTENTS

CHAPTER 1	
BACKGROUND	1
<hr/>	
1.1 Introduction	1
1.2 Summary of work	1
1.3 Theory of fan acoustics	3
1.4 Bands	5
1.5 A-weighted sound level	6
1.6 Digital signal processing	7
1.6.1 Fast Fourier transform (FFT)	7
1.6.2 Acoustic pressure	9
1.6.3 Subtracting the mean	10
1.6.4 Cosine taper window	10
1.6.5 Averaging	11
1.6.6 Synchronized signals	11
1.6.7 Electrical noise	12
CHAPTER 2	
EQUIPMENT	13
<hr/>	
2.1 Anechoic chamber	13
2.1.1 Construction	13
2.1.2 Qualification	15
2.2 Data acquisition equipment	18
2.2.1 Microphone	18

2.2.2	DAQ Board	19
2.2.3	Optical Sensor	19
2.2.4	LabVIEW	19
2.2.5	PC	19
2.2.6	SETUP	20
CHAPTER 3		
FAN ACOUSTIC MEASUREMENTS		21
<hr/>		
3.1	Unducted fan	21
3.1.1	Fan acoustics	21
3.1.2	Beam pattern	22
3.2	Ducted Fan	25
CHAPTER 4		
FAN NOISE CONTROL		27
<hr/>		
4.1	Active control	27
4.2	Passive Control	35
CHAPTER 5		
AXIAL FORCE MEASUREMENT		37
<hr/>		
5.1	Static force calculation	37
5.2	Dynamic force calculation	38
5.3	Magnetic force in motor	40
5.4	Measurement apparatus	41
5.4.1	Design 1 – strain gage	41
5.4.2	Design 2 – accelerometer	46

5.4.3	Design 3 – pulleys	50
5.4.4	Design 4 – silicon / Teflon	52
5.5	Conclusions	54
5.6	Recommendations for future work	55
REFERENCES		56
<hr/>		
APPENDIX		58
<hr/>		
A1.	Strain gage	58
A2.	Fan properties	59
A3.	Cantilever properties	61
A4.	Silicon roughness	62
A5.	Photographs	63
List of Tables		67
List of Figures		67



CHAPTER 1

BACKGROUND

1.1 Introduction

The Air Conditioning and Refrigeration Center (ACRC) is a National Science Foundation Industry/University Cooperative research center aimed at providing the technology base for a new generation of energy-efficient, quiet, and reliable equipment that can use environmentally safe refrigerants. About 20 sponsoring companies donate resources and funds so that pre-competitive research can be performed by graduate students, faculty members, undergraduate students, and visiting scholars. Research is focused on the questions most important for system design and performance (ACRC, 1999). For more information about the ACRC, visit the Center's web site at <http://acrc.me.uiuc.edu>.

Project 84 concentrates on noise generating mechanisms of axial-flow fans with the intent of proposing methods of component design and system assembly by which noise generation is reduced or minimized. The project consists of three parts: theory of fan acoustics, fan noise generation as a function of spatially non-uniform inflows, and the correlation of fan acoustics with fan shaft dynamic axial force.

1.2 Summary of work

- Built and qualified an anechoic chamber according to ANSI and ISO standards.
- Obtained a microphone and other required acoustic data acquisition equipment.

- Learned how to use graphical programming and data analysis software – LabVIEW. Have written several VIs, primarily one that obtains an acoustic signal, FFTs it, and calculates octave band sound levels and the A-weighted sound level.
- Measured the beam pattern of the fan at the blade passage frequency. It resembles dipole radiation as expected – but not perfectly, why?
- Built a plastic duct with throttling capability in order to control inlet flow into the fan. Measured acoustics vs. varying inlet conditions – antisymmetric obstructions, flow straighteners, etc. Studied the acoustic effects of tip clearance, fan eccentricity, and various heat exchanger fin geometries. (KD SMITH)
- Obtained a hotwire anemometer and a pressure transducer to obtain flow measurements in the duct.
- Considered building a Mylar box (according to INCE standards) and also a Mylar duct. Mylar is acoustically transparent – eliminate duct resonance. Idea on hold.
- Experimentally determined fan blade stiffness (load-deflection curve), blade weight, and dimensions, with help of Prof. A.J. Paris, so that R. Weaver could estimate the natural frequency of the blade. Attached an accelerometer to the blade to make dynamic response measurements.
- Considered R. Weaver’s idea of altering the axial stiffness of the fan shaft in order to reduce or eliminate acoustic radiation at the blade passage frequency. Idea on hold.
- Found work by MacGillivray *et al* at Penn State → Actively shaking an axial fan, periodically in the axial direction, can significantly reduce acoustic emission at the BPF and some harmonics. Future work may involve repeating their work.

- Conducting a study of the correlation between dynamic axial force in the fan shaft and acoustic emission at the BPF. Building a device that measures dynamic axial force in the shaft using a cantilever and accelerometer. (SE ZELLER)

1.3 Theory of fan acoustics

Fan acoustic theory is based upon the aerodynamic sound generation principles laid out by M.J. Lighthill and N. Curle in the mid 1950s and also by Ffowcs Williams and Hawkins. Lighthill developed a theory in which the intensity of the sound produced by a moving fluid can be predicted. Curle extended Lighthill's work to include the presence of solid boundaries in the flow.

There are three mechanisms (sources) by which acoustic energy can be generated. A monopole source consists of mass fluctuating in a fixed region of space. A dipole source consists of momentum fluctuating in a fixed region of space, or varying rate of mass flux across a fixed surface. A quadrupole source consists of varying the rate of momentum flux across a fixed surface, or sound generated by externally applied stress. Lighthill showed that sound generated aerodynamically is quadrupole in nature. Curle showed that when solid boundaries are present in a flow, a dipole generation mechanism is added. He also showed that the dipole mechanism dominates over the quadrupole mechanism.

These three sound generation mechanisms can be applied to fan noise¹. Monopole noise is generated by volume displacement effects created by moving fan blades. Fluctuating forces acting between the flow and the fan blades generate dipole noise. Quadrupole

noise is also present due to Lighthill's fluctuating shear forces in the flow. Monopole and quadrupole noise are both weak compared to dipole noise.

The fluctuating forces acting between the flow and the fan blades, which result in dipole noise generation, can be either steady forces or unsteady forces. Steady forces result in what is called "Gutin" noise. Steady forces occur when a fan operates in a uniform, steady flow field. "Gutin" noise is discrete, occurring at the blade passage frequency² (BPF) and its harmonics. Unsteady forces occur when a fan operates in a steady but spatially non-uniform flow field. Each fan blade experiences an unsteady force as it passes through the non-uniform region of flow. Discrete dipole noise is generated at the BPF and its harmonics. Spatially non-uniform flows are generated by wakes from upstream obstructions in the flow. Usually, "Gutin" noise is negligible compared to noise generated by unsteady forces.

Non-uniform unsteady flows, secondary flows, vortex shedding, and turbulent boundary layers all also generate dipole noise. However, in these cases the noise is broadband rather than discrete. The chart in Figure 1 summarizes fan noise generation mechanisms.

¹ Fan acoustic theory is taken primarily from the review paper by W. Neise

² The blade passage frequency equals the fan revolution frequency times the number of blades.

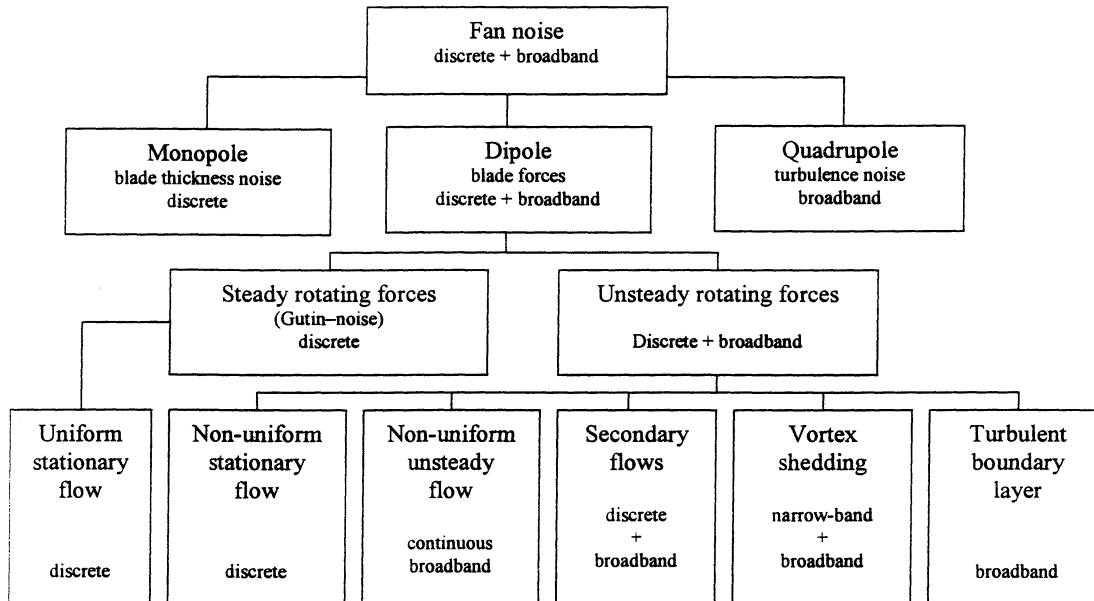


Figure 1. Fan noise generation mechanisms (Neise, 1992)

1.4 Bands

- Sound is complex, not of a single frequency. Often, the over-all sound pressure level (SPL) is not needed. Instead SPL vs. frequency is desired. This is obtained by using a band-pass filter whose mid-band frequency is continuously or step-wise variable. This allows sound pressure to be measured in known bands of frequencies.
- There are three types of analyzers: constant bandwidth, constant % narrow bandwidth, and octave, 1/2-octave or 1/3-octave bandwidth.³

³ Notes from *Acoustics*, Leo Beranek, p362

- Apparent loudness of sound varies not only with pressure but also with frequency (pitch). The way it varies with frequency depends upon the sound pressure.
- When a weighting characteristic is used, the reading is said to be a “sound level” (SL) as opposed to a “sound pressure level”
- Octave bands: $f_{\text{upper}} = 2f_{\text{lower}}$. Typical center frequencies are 31.5, 63, 125, 500, 1000, 2000, 4000, 8000, 16000.
- 1/3-octave bands: split octaves into three parts for a more detailed analysis. Center frequencies would be, for example, 100, 125, 160, 200, 250, 315, 400, 500, 630, 800...⁴

1.5 A-weighted sound level⁵

The overall SPL is not always a desired quantity because most of the acoustic pressure could be at a frequency that is outside of the range detectable by the human ear. An A-weighted sound level is one in which weights are assigned to pressures according to frequency. Sounds occurring at frequencies most audible by humans receive the highest weights. The resulting sound level is still a single number, the A-weighted SL in dBA.

A frequency-band analysis can be converted into an A-weighted SL using charts that have been created for this purpose. At each band level there is a correction factor in dB to be added. This new value is converted from dB to a relative power. Then the relative powers of all center frequencies are summed, and the sum is converted back into a dB

⁴ Notes from *Handbook of Noise Measurement*, 7th ed. A Peterson and E. Gross Jr.

⁵ For more information on A-weighting, see p.77, Ap I, Ap II, in *Handbook...* or see *Fundamentals of Acoustics*, 3rd ed. Kinsler, Frey et al. 1982.

level, which is the corresponding A-weighted SL for that band analysis (Kinsler, 1982).

An A-weighted analysis is less detailed than a frequency-band analysis.

1.6 Digital signal processing

Data is acquired digitally by the data-acquisition board. The user specifies the sample rate (samples/second) and number of samples through a graphical programming software package called LabVIEW.

1.6.1 Fast Fourier transform (FFT)⁶

The relationship between a waveform in the time domain and its representation in the frequency domain is established by the Fourier transform (FT). The Fourier transform $X(f)$ of a waveform $x(t)$ is given by

$$X(f) = F(x(t)) = \int_{-\infty}^{\infty} x(t)e^{-j2\pi ft} dt.$$

The inverse Fourier transform is given by

$$x(t) = F^{-1}(X(f)) = \int_{-\infty}^{\infty} X(f)e^{j2\pi ft} dt.$$

The discrete representation of the Fourier transform is derived by sampling the Fourier transform pair $x(t) \Leftrightarrow X(f)$ using the following relationships:

$$\Delta t = \frac{1}{f_s} \Delta f = \frac{f_s}{n},$$

⁶ Notes from LabVIEW Help.

where Δt is the sampling interval, Δf is the frequency resolution, f_s is the sampling frequency, and n is the number of samples in both the time and frequency domain.

The discrete transform pair $x_i \leftrightarrow X_k$ is obtained, and the discrete Fourier transform is given by

$$X_k = \sum_{i=0}^{n-1} x_i e^{-j2\pi k i / n} \Delta t.$$

the inverse is given by

$$x_i = \sum_{k=0}^{n-1} X_k e^{j2\pi k i / n} \Delta f.$$

The amplitude spectral density is given by X_k . The amplitude spectrum is determined by multiplying the RHS by Δf :

$$X_k = \sum_{i=0}^{n-1} x_i e^{-j2\pi k i / n}$$

for $k = 0, 1, 2, \dots, n-1$

$$x_i = \frac{1}{n} \sum_{k=0}^{n-1} X_k e^{j2\pi k i / n}$$

for $i = 0, 1, 2, \dots, n-1$.

The discrete Fourier transform (DFT) is computed using an algorithm called the FFT.

The units of the FT are volts-sec. The units of the FFT are volts. A FFT plot can be transformed into a FT plot by multiplying the FFT by Δt . Also, the FFT is an array of

amplitudes vs. index numbers. To convert index number to frequency, use the following relationship:

$$f = \frac{\text{indexnumber}}{\text{totaltime}}$$

1.6.2 Acoustic pressure

After computing the FFT of a digitally acquired acoustic signal, the rms acoustic pressure p_{rms} over a band of interest can be determined from the following derivation:

T = total time of sampling

B = 1 over band of interest. 0 over all other frequencies

df = $\delta f \cdot \text{index}$

n = # of samples

$n \cdot \delta t / T = 1$

V = voltage

ω = angular frequency

$$\frac{V^2_{rms}}{\text{band}} = \frac{1}{T} \int |B * V(t)|^2 dt = \frac{1}{2\pi T} \int |\tilde{B}(\omega)|^2 |\tilde{V}(\omega)|^2 d\omega$$

$$\tilde{V}(\omega) = \delta t \int e^{-i\omega t} V(t) \frac{dt}{\delta t} = \delta t \sum_t V(t) e^{-i\omega t} = \delta t \cdot FFT$$

so

$$\frac{V^2_{rms}}{\text{band}} = \frac{1}{2\pi T} \delta\omega \int |\tilde{B}(\omega)|^2 (\delta t)^2 |FFT|^2 \frac{d\omega}{\delta\omega} = \frac{\delta\omega}{2\pi T} (\delta t)^2 \sum |\tilde{B}(\omega)|^2 |FFT|^2$$

$$\delta\omega = \frac{2\pi}{T}, \quad B = 1 \text{ over band,}$$

$$V^2_{rms} = \frac{2\pi(\delta t)^2}{2\pi T^2} \sum_{\text{band}} |FFT|^2 = \frac{2}{n^2} \sum_{\text{band}} |FFT|^2, \quad \left(\frac{\text{multiply by 2 because sum is over}}{\text{negative and positive frequencies}} \right)$$

The rms voltage is converted into rms pressure via the calibration constant for the microphone. The constant for the mic used in this project is 13.3 mV/Pa. So the rms pressure over a band of interest is

$$p_{rms} = \left[\frac{2}{n^2} \sum_{band} |FFT|^2 \right]^{1/2} \cdot \frac{1}{13.3 mV / Pa}.$$

The sound level for the band is then computed from

$$SL = 20 \log \left(\frac{p_{rms}}{p_{ref}} \right) = 20 \log \left(\frac{p_{rms}}{20 \mu Pa} \right).$$

1.6.3 Subtracting the mean

Subtract the mean of the signal to eliminate DC offset. This can be done by summing all values of the signal, dividing by the total number of samples, and subtracting that value (the mean) from every value in the signal.

1.6.4 Cosine taper window

Passing the signal through a cosine taper window before analyzing it gets rid of a lot of junk in the FFT. However, a correction factor must be applied to octave band SLs to account for the energy lost in the taper. The correction factor is $\log_{10} \langle w^2(t) \rangle$. For a loss of 5% on both sides, the correction factor is $20 \log_{10}(1/.9) = 20 \log_{10}(1.111) = 0.91515$ dB.

1.6.5 Averaging

Some type of averaging may be required in order to obtain repeatable results. Several averaging techniques will now be discussed.

One solution is to obtain a very large number of samples. However, calculations such as the FFT will take a lot of time to compute, given such a large number of samples.

Averaging a certain number of neighboring points into a single point can solve this problem. For example, take the first four points and average them to become the first point. Then take the next four points (points 5-8) and average them to become the second point, etc. The number of samples is reduced by a factor of four.

One way to obtain repeatable octave-band SLs is to analyze many small sets of data and average the resulting SLs. Another way is to average many small FFTs and then calculate the octave-band SLs.

1.6.6 Synchronized signals

When averaging signals, it is a very good idea to use synchronized signals so that random and background noise can be minimized. Synchronized signals can be obtained by triggering data acquisition from some known reference point. For example, in fan acoustic measurements, data acquisition should begin at the same fan blade position every time. An optical sensor can be used to sense blade position.

1.6.7 Electrical noise

To avoid electrical noise, keep wires that send signals to the computer away from other wires of higher voltage. Also, unbalanced wires, wires that are grounded more than once, can be a source of electrical noise because a difference between the grounds induces current flow, which the DAQ board will detect. Use balanced cables if possible, or use only one ground. Only shield a cable at one end. Poorly grounded building power can also be a source of electrical noise (Schomer, 1999).

CHAPTER 2 EQUIPMENT

2.1 Anechoic Chamber

2.1.1 Construction

An anechoic chamber was designed (dimensions and cutoff frequency). Prefabricated components were purchased, and the room was assembled. The components consist of sound-insulating walls (steel shell with sheet rock and insulation inside), foam wedges, a steel grated floor, and posts upon which the floor rests. The chamber occupies about 75% of room 357, Mechanical Engineering Lab. The walls extend from floor to ceiling. Wedges are glued (with Liquid Nails) to all walls, the ceiling, and the floor. The posts are bolted to the floor and extend up through, and just above, the wedges. The grated floor rests on the posts. The interior dimensions are 7' x 10' x 7'. The cutoff frequency is approximately 250 Hz. A photograph of the chamber is given in Figure 2.



Figure 2. Anechoic chamber

2.1.2 Qualification

In order to ensure that the anechoic chamber is truly anechoic, it has undergone a series of tests using procedures given in ANSI S12.35-1990 and ISO 3745 Standards as guides. A variable-frequency horn, controlled with a waveform generator and amplified by 20dB with a filter/amp, was placed on the chamber floor at the center of the back wall. Sound pressure measurements were taken at varying distances along four different paths, all beginning at the center of the horn and moving away from it in straight lines but at varying angles. Path #1 is straight on axis (of the horn). Path #2 is diagonal to the upper RH corner, at the opposite end of the chamber. Path #3 is diagonal to the upper LH corner, at the opposite end of the chamber. Path #4 is straight up from the horn, now located in the center of the chamber floor. Acoustic measurements were taken at about 10 locations along each path. At each location, the horn was operated at 250, 500, 1000, and 2000 Hz, and measurements were taken at each frequency. The sound levels of 1/3-bands centered at these frequencies were plotted versus the log (base 10) of the distance away from the horn along the path. According to theory, the sound level should decrease proportionally to the inverse square of the distance away from the source. So a slope of -20 dB suggests that the room is truly anechoic. The qualification plots are given in Figures 3 through 6.

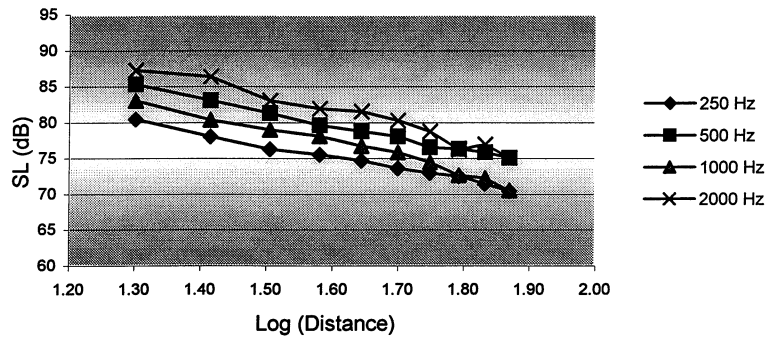


Figure 3. Qualification: Path #1 – On axis

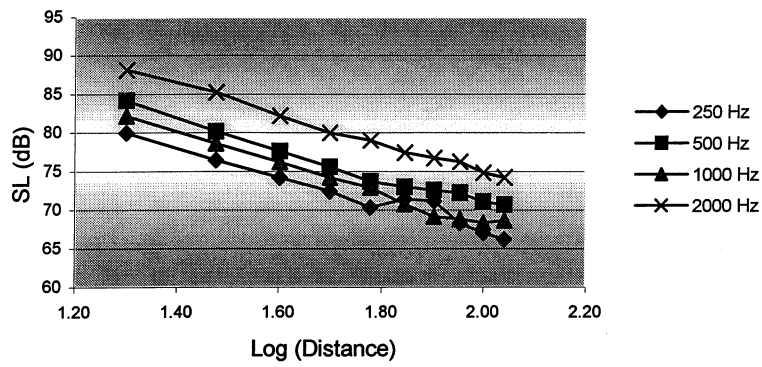


Figure 4. Qualification: Path #2

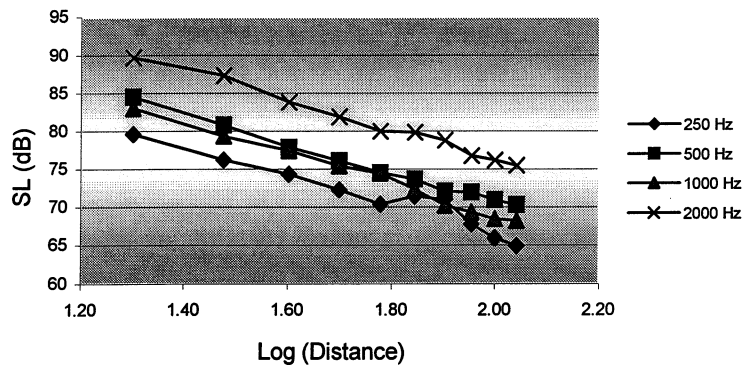


Figure 5. Qualification: Path #3

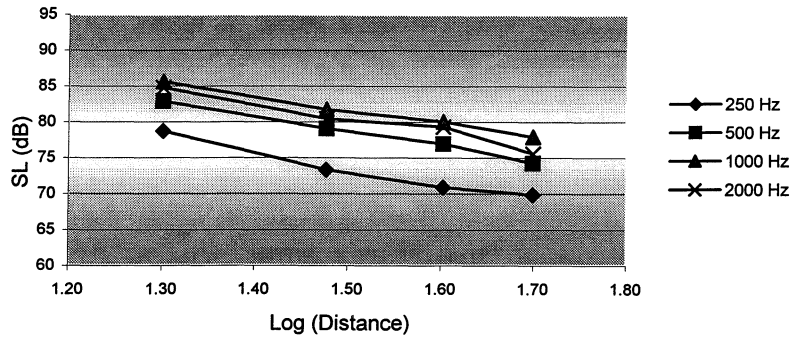


Figure 6. Qualification: Path #4 – straight up

According to the standards, deviations from the inverse-square law should be no more than ± 1.5 dB for frequencies < 630 Hz and > 6300 Hz and no more than ± 1.0 dB for frequencies between 630 Hz and 6300 Hz. In order to determine the deviations for the data plotted above, the SL measurements were normalized with respect to distance, and the deviations (difference between normalized value and the average normalized value) were calculated. The results are given in Tables 1 through 4. Deviations that exceed the requirements are shown in bold.

Table 1. Path #1 Deviations

Log (distance)	250 Hz deviation	500 Hz deviation	1000 Hz deviation	2000 Hz deviation
1.30	-0.89	-0.44	0.00	-0.26
1.41	-1.00	-0.37	-0.38	1.16
1.51	-1.01	-0.34	0.04	-0.41
1.58	-0.23	-0.53	0.63	0.02
1.64	0.17	-0.11	0.53	0.89
1.70	0.23	0.27	0.77	0.76
1.75	0.52	-0.27	-0.34	0.21
1.79	0.99	0.40	-0.57	-1.42
1.83	0.74	0.71	-0.15	0.09
1.87	0.45	0.71	-1.19	-1.07

Table 2. Path #2 Deviations

Log (distance)	250 Hz deviation	500 Hz deviation	1000 Hz deviation	2000 Hz deviation
1.30	-0.96	-0.09	0.03	-0.45
1.48	-0.96	-0.56	-0.04	0.19
1.60	-0.69	-0.64	0.03	-0.36
1.70	-0.55	-0.73	0.00	-0.65
1.78	-1.05	-1.02	0.31	-0.02
1.85	1.36	-0.38	-0.53	-0.25
1.90	2.26	0.39	-1.00	0.18
1.95	0.41	1.02	-0.29	0.71
2.00	0.08	0.81	0.18	0.22
2.04	0.05	1.23	1.28	0.44

Table 3. Path #3 Deviations

Log (distance)	250 Hz deviation	500 Hz deviation	1000 Hz deviation	2000 Hz deviation
1.30	-0.95	0.07	0.04	-0.44
1.48	-0.83	-0.13	-0.11	0.69
1.60	-0.21	-0.54	0.45	-0.32
1.70	-0.31	-0.38	0.40	-0.29
1.78	-0.66	-0.37	0.95	-0.65
1.85	1.75	0.07	0.20	0.57
1.90	2.42	-0.34	-0.77	0.67
1.95	0.26	0.53	-0.63	-0.34
2.00	-0.64	0.44	-0.58	-0.04
2.04	-0.84	0.64	0.04	0.14

Table 4. Path #4 Deviations

Log (distance)	250 Hz deviation	500 Hz deviation	1000 Hz deviation	2000 Hz deviation
1.30	1.12	0.20	-0.11	0.37
1.48	-0.73	-0.08	-0.44	-0.46
1.60	-0.67	0.31	0.36	0.95
1.70	0.28	-0.44	0.20	-0.85

2.2 Data Acquisition Equipment

2.2.1 Microphone

The microphone is a ½ inch MK 202 condenser cartridge designed for acoustic measurements in research and industry. The frequency range is up to 40 kHz, free field, at SPLs up to 158 dB. The sensitivity is 13 mV/Pa. The preamplifier is a MV 203 high-

impedance (20 GOhm) transducer. The power supply is a MN900 two-channel unit, which supplies an operating voltage of 120V to the preamp and a polarization voltage of 200V to the mic. All components were made by Microtech Gefell GMBH, Germany and distributed by Josephson Engineering, San Jose, CA.

2.2.2 DAQ board

The data acquisition (DAQ) board is a *National Instruments* AT-A2150 dynamic signal acquisition board for the IBM PC and compatible computers. The board has 4 channels of 16-bit, simultaneously sampled analog input and can sample at rates up to 48 kHz.

2.2.3 Optical sensor

A *Monarch* ROS-5P Remote Optical Sensor is used to detect fan speed and blade position. The sensor emits a visible red LED and senses reflected pulses from a reflective tape target. Power is supplied to the sensor by a *Monarch* SPS-5 Self-Powered Sensor.

2.2.4 LabVIEW

All data acquisition and analysis is controlled and performed using LabVIEW, which is a graphical programming software package made by *National Instruments*. LabVIEW allows for the creation of programs called virtual instruments (VIs), which look and operate like real instruments (oscilloscopes, voltmeters, frequency analyzers, etc.).

2.2.5 PC

The DAQ board and LabVIEW software are installed in a *Dell* Windows 95 PC equipped with a Pentium II processor.

2.2.6 Setup

Acoustic data is taken in the anechoic chamber with the microphone. The signal is passed from the mic/preamp to the power supply and then to the DAQ board located inside the PC. Data acquisition is controlled by the user through LabVIEW. A diagram of the setup is given in Figure 7.

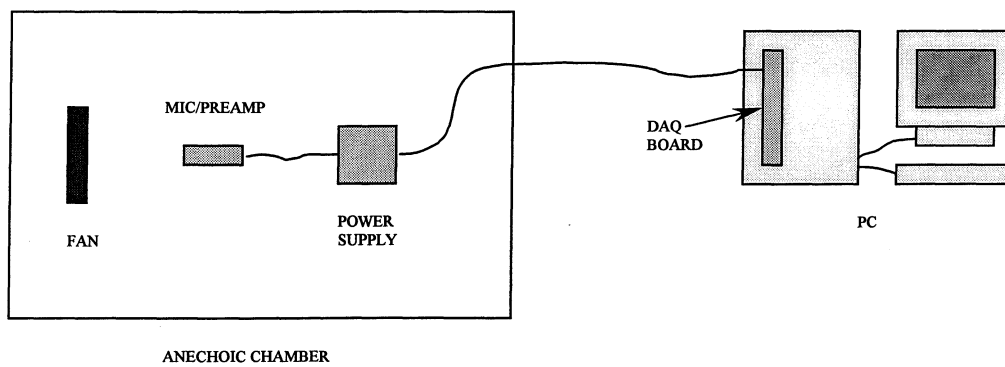


Figure 7. Setup

CHAPTER 3

FAN ACOUSTIC MEASUREMENTS

3.1 Unducted Fan

3.1.1 Fan acoustics

Examination of the Fourier Transform of a fan's acoustic signal can provide some insight in terms of the sound generating mechanisms present. For example, uniform and non-uniform stationary flows and secondary flows all create discrete noise, which appears in an FFT as a sharp peak at a particular frequency (or frequencies). Non-uniform unsteady flows, vortex shedding and turbulent boundary layers all create broadband noise, which appears in an FFT as a response occurring over a wide range of frequencies.

The Fourier transform of an acoustic signal from the 4.375" diameter, 5-bladed fan used in this research is given in Figure 8. Note the sharp peaks at the blade passage frequency (revolution speed x number of blades) and its multiples. Discrete noise at these frequencies is generated by stationary flows. The FFT of the signal from the optical sensor is also shown; it confirms the revolution frequency of the fan.

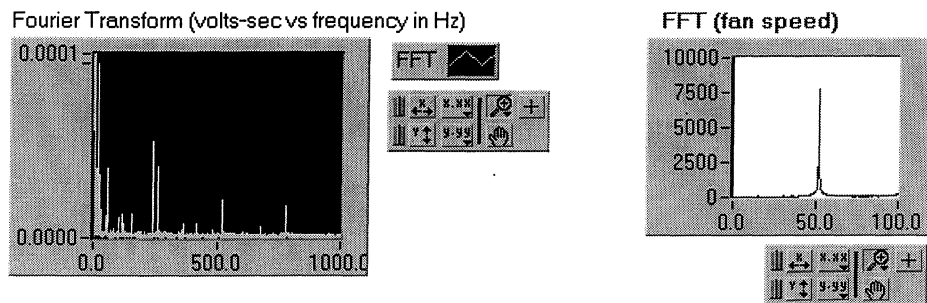


Figure 8. Acoustic frequency response of 5-bladed fan

3.1.2 Beam pattern

A beam pattern (or directivity plot) shows the pressure amplitude (or sound level) distribution as a function of angular position at a fixed radius from an acoustic source. For axial fans, the main cause of noise at the BPF and its harmonics is the fluctuating forces between the air and the fan blades. This type of sound generating mechanism produces dipole radiation. The beam pattern for perfect dipole radiation is given in polar representation in Figure 9.

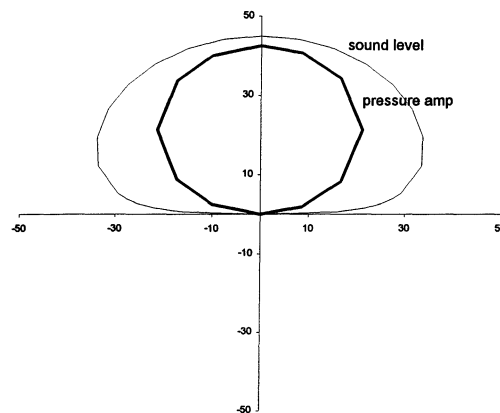


Figure 9. Theoretical dipole beam pattern

Many beam pattern measurements were made of a 5-bladed, 4.375" diameter, plastic, refrigerator compressor cooling fan. The measurements were made in the anechoic chamber with the microphone described previously. The mic was attached to an adjustable mic stand, and, in most cases, the fan remained stationary while the mic was traversed along a semicircular path in the x-z or y-z plane (z being in the direction of the fan axis). In some cases, the mic position was fixed, and the fan was rotated. Results are given in Figures 10 through 12.

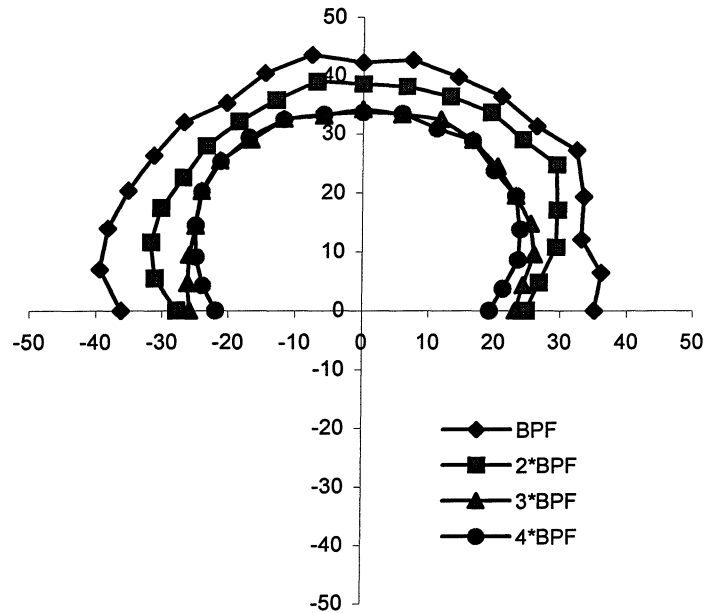


Figure 10. Directivity SPL(dB) of fan at BPF and harmonics, $r = 52''$
(4-point averaging using 4-pt avg.vi)

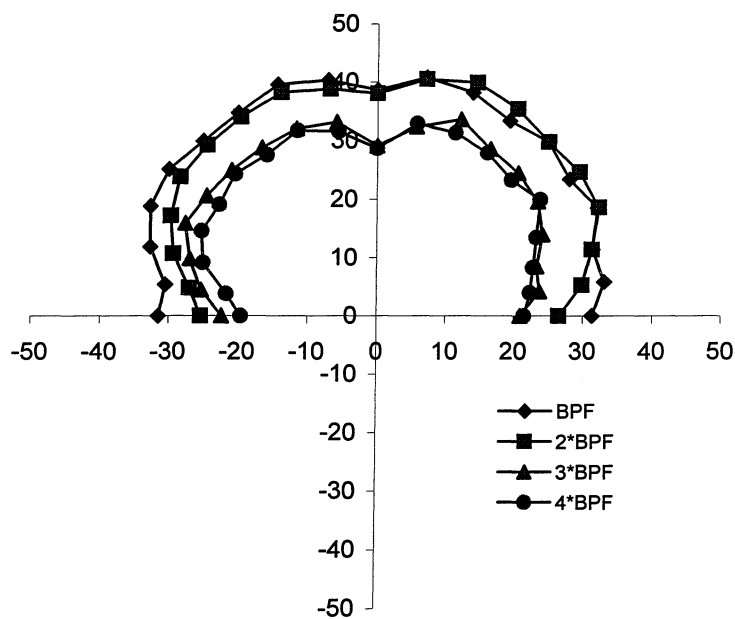


Figure 11. Directivity SPL(dB) of fan at BPF and harmonics, $r = 38.75''$
 (avg. FFT of 10 synchronized acquisitions using AvgFFT.vi)
 (48,000 samples – 16,000 sa/sec)

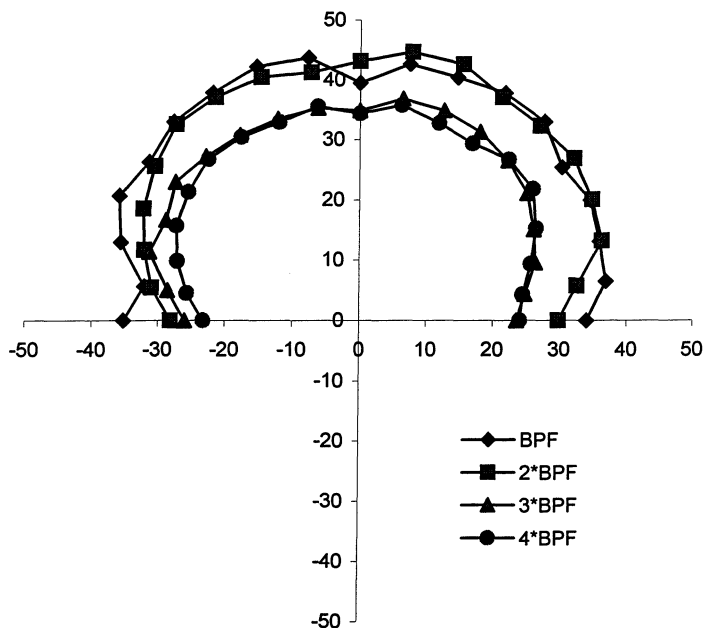


Figure 12. Directivity SPL(dB) of fan BPF and harmonics, $r = 38.75''$
 (avg SL of 10 synchronized acquisitions using SyncBPFAvgdB.vi)
 (48,000 samples – 16,000 sa/sec)

3.2 Ducted Fan

A duct test section was designed for the 4.375" diameter fan. It has a bellmouth and a conically-shaped valve that is used to throttle the flow. The inflow uniformity is controlled by flow straighteners (drinking straws) and screens inside the duct. The duct can be taken apart in sections so that blockages and obstructions can be easily inserted into the flow. A drawing of the test section is given in Figure 13.

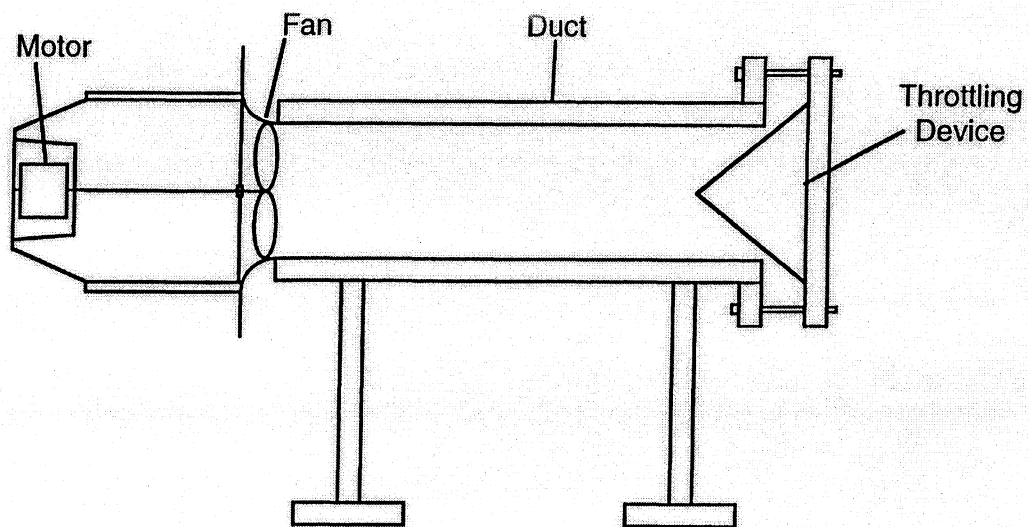


Figure 13. Duct test section (courtesy of K.D. Smith)

Several differently-shaped obstructions were placed in the duct, upstream of the fan, in order to create a spatially non-uniform inflow. Hot-wire anemometry and a pressure transducer were used to obtain the flow field characteristics in the duct. Acoustic measurements were made at varying obstruction locations in order to obtain a relationship between inflow non-uniformity and acoustic radiation.

Other studies conducted with the test section include how fan noise is affected by blade tip clearance, fan eccentricity, and different heat-exchanger fin geometries. Detailed information about the tests conducted in the duct test section can be found in the ACRC extended summary of Project #84 for Fall 1999 and in the master's thesis by K.D. Smith.

CHAPTER 4

FAN NOISE CONTROL

4.1 Active control

An active fan noise control study was done at Penn State Univ. by J.R. MacGillivray, G.C. Lauchle, and D.C. Swanson. This section contains notes from publications of their work and also from several of their relevant references.

Notes from “Active control of axial-flow fan noise”, G.C. Lauchle, J.R.

MacGillivray, D.C. Swanson.

Summary

- Shake a fan axially with an electrodynamic shaker
- Use a NEAR FIELD mic as an error sensor
- Use a tachometer to obtain a reference signal
- Use a baffled fan unit (small, commercial, electronic cooling fan) operating in free field
- A cylindrical flow obstruction is placed on the inlet side
- Reduced SPL at BPF by 20 dB
- Reduced 2nd and 3rd harmonics by 15 and 8 dB
- A cabinet enclosure over fan did not affect results

Feasibility

- Can a shaken fan radiate sound with a reasonable power input?

- Is the directivity pattern of a shaken fan equal to the directivity pattern of an operating fan?
- A 7-bladed, 82mm dia, Nidec plastic fan was placed in a flow-through anechoic chamber. An aluminum disk on the back of the frame connected to a Wilcoxon F3 shaker via a stinger of SSSL rod. The fan axis was oriented vertically above anechoic wedges. The fan was un baffled.
- The fan was shaken at 264 Hz, which was the operational BPF (is it rotating too?)
- It was found that the shaken fan can produce more sound than the fan in free operation – it can be an antinoise source.
- When the flow was directed toward the mic (located 1 m away), the shaken fan acoustic pressure dropped by 2 dB (as opposed to directing flow away from mic – placing mic upstream). According to ref 14, this is due to a change in radiation impedance caused by the flow.

Directivity Patterns

- Directivity measurements were made by placing the mic 1 m away from the fan, attaching it to a boom, and taking measurements at 5° increments. In order to obtain repeatable results, over 300 data sets were taken, their FFTs squared and added, then averaged.
- Skewed directivity patterns were obtained. More info about such patterns can be found in refs 8 (Quinlan), 12, and 13.
- When the fan was placed in a baffle, a monopole directivity pattern was obtained. (Measurements were made on the inlet side of the fan. A nearly identical pattern was

obtained for the outlet side) Since a shaken fan is expected to have peak SPL on axis, a baffled fan should be most efficient for noise cancellation.

Setup

- The mic was placed on the inlet side, one fan diameter or more away. The tachometer (optical sensor) was also placed on the inlet side. Reflective tape strips were placed on the leading edge of each blade. The fan was placed in a plywood baffle, its inlet side flush with the baffle. There was a 5mm gap between the fan housing and the baffle. A rod was placed across the center of the fan at about 0.1 radius axially from the hub (for more info on rod obstruction, see ref 17, Washburn).

A diagram of the setup is given in Figure 14.

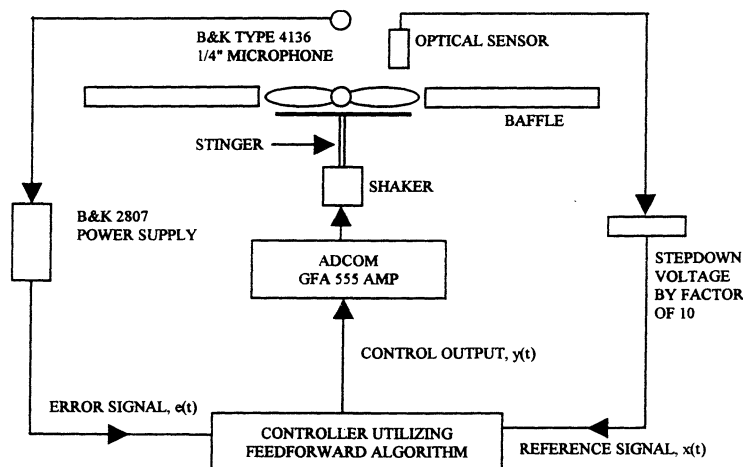


Figure 14. Setup (G.C. Lauchle, J.R. MacGillivray, D.C. Swanson)

- The sound power was measured over a 0.5 m diameter hemisphere.

Results

- Reductions in sound pressure and sound power were observed. The pressure reduction was greater than the power reduction because of directivity patterns.
- A null along the fan axis shows that shaking almost completely cancels the sound.
(*but there is a null when the shaker is off!)
- Reductions on the outlet side were achieved but were not as great.

Future work

- Internal force sensor (ref 20 – same as ref 19)
- Shake rotor only
- Multiple shakers – shake individual blades

Notes from Ref 9: “Subsonic axial flow fan noise and unsteady rotor force”, Wen-Shyang Chiu, G.C. Lauchle, and D.E. Thompson.

Summary

- Used coherence function measurements to show radiation at first several harmonics of the BPF is due entirely to the integrated unsteady rotor force

Objective

- Correlate inflow non-uniformity, unsteady blade loading, and discrete-frequency radiated noise

Setup

- Used a typical electronic/computer cooling fan – 18 cm diameter
- Placed a small cylinder in the inflow

Correlation of discrete-frequency (DF) noise and unsteady rotor force

- Operated the fan at minimum static pressure rise in order to maximize DF noise – no obstructions and with cylinder obstruction.
- A force sensor was placed between the rotor and the root of the shaft in order to measure to total (integrated) unsteady rotor axial force. The sensor was a piezoceramic transducer with a silver coating to shield from the motor's magnetic field.
- The acoustic pressure at the mic due to fluctuating force on the rotor was determined using complex coherence functions and the coherent output spectrum between the measured shaft force and radiated sound pressure (?).

Measurement of time-invariant spatial inflow velocity

- Miniature, 5-hole probes, which can measure flow angle and velocity, were placed on a rotating unit with 3-degree increments.
- Fig 10 shows the circumferential velocity caused by the wake from the cylinder.
- Fig 11 shows the secondary inflow velocity

Computation of discrete-tone radiated sound

- Decomposed spatially non-uniform inflow velocity into a sum of sinusoidally-varying components with various amplitudes and frequencies – sinusoidal variation in blade loading occurs.
- Based on geometry, unsteady rotor force was computed using CFD.
- The DF noise was computed using a dipole source model – Curle’s generalized solution of Lighthill’s equation, simplified with assumptions:
 - Low blade tip Ma
 - Blade surface in rigid, steady motion
 - Total blade force dominated by normal component

$$p(r, t) \cong \frac{\cos \theta}{4\pi r} \left(\frac{\partial F}{\partial t} \right) \cong \left(\frac{f \cos \theta}{4\pi r c_o} \right) F(f) \quad (p647)$$

- Sound wavelength > fan diameter (compact source)
- Compared predicted radiated noise to measured radiated noise. (Why not just use force sensor to predict noise?) Computed and measured agree at BPF and first harmonic but not at higher harmonics (at which the source is less compact and the equation does not apply).

Notes from Ref 8: “Application of active control to axial flow fans”, D.A. Quinlan.

Summary

- Discussion of skewed directivity patterns and active control methods for tonal radiation of axial fans

Directivity measurements

- Rotated the fan axially relative to a stationary mic, in 5-degree increments.
- No baffle
- Took minimum and maximum amplitudes over 5-second periods at each angle and frequency in order to obtain and compare “max” and “min” directivity patterns
- The pattern at the BPF had a defined shape with a null, while the pattern from the broadband components had an undefined shape. This implies that the generating mechanisms are inherently different.
- At the BPF, sources within the fan are coherent – compact source.
- At broadband components, noise is generated by a distribution of uncorrelated acoustic sources – can’t use a dipole configuration to attenuate broadband noise.
- The cause of skewness of tonal directivity is not known. Maybe there is a slight azimuthal variation in blade-tip clearance.

Sound cancellation

- Placing two identical, out-of-phase fans side by side won’t work because the amplitude of the tones is time-dependent (variations of 5 dB are caused by large-scale eddies in the flow environment).
- A loud-speaker is used instead. Noise reduced by 12 dB at the BPF and by 10 dB A-weighted.

Notes from Ref 17: “Inlet flow conditions and tonal sound radiation from a subsonic fan”, Karl B. Washburn and G.C. Lauchle.

Summary

- An empirical survey of tonal noise generated by a small axial cooling fan operating in the presence of upstream obstructions.

Observations

- A rod was placed across the center of the fan at $0.1R$ axially from the hub
- The steady lift on the blades contributes most to the BPF (Gutin noise)
- The unsteady blade loading by fluctuating lift on the blades as they pass through time-invariant, non-uniform inflow contributes to BPF but is the dominant contributor to higher harmonics.

Design recommendations

- Aerodynamically shape obstructions
- Place obstructions at least 0.3 fan radii from inlet
- Avoid blockage of lateral inflow
- Increase the number of blades and blade solidity in order to optimize aerodynamics for lowest tip-speed fan possible
- Reduce fluctuating forces on blades by removing obstructions, etc.

Conclusions

- DF noise is caused by the “propeller mechanism” and by periodically fluctuating aerodynamic force regions.
- The “propeller” noise is the result of steady loading on each blade as a function of fan operating point.
- Other DF noise is the result of a spatially non-uniform, time-invariant velocity field. Sound is radiated as dipoles.
- If the BP tone-levels do not vary with inflow distortions, propeller noise is the dominant source.
- With a cylinder in the inflow, BPF does not decrease with increased separation like the higher harmonics do. This is because wake interaction is not a dominant source of energy at the BPF. (So if non-uniformities are the cause of tonal radiation, and it occurs at harmonics of the BPF, why does active control have the greatest effect at the BPF?)

4.2 Passive control

It may be possible to decrease axial fan noise passively by making the fan shaft flexible such that the fluctuating axial forces on the fan blades are eliminated. In other words, the shaft flexibility allows the fan blades to move axially with a velocity that is equal to the velocity of the air hitting the blades. So the blades are “avoiding” the forces generated by spatially non-uniform inflow, and the noise that would have been generated by these forces is eliminated.

This idea was explored theoretically. It was determined that the required Q (inverse of damping) for the system would be too high, and the idea was abandoned for now.

CHAPTER 5

AXIAL FORCE MEASUREMENT

5.1 Static force calculation

A fan operating in a duct with steady, spatially-uniform flow will experience a static axial force, or thrust, which is constant. The equal-and-opposite force required to anchor the fan is in the direction of air flow (the fan wants to move in the direction opposite to the direction of flow). This static force is calculated by applying conservation of linear momentum. A diagram of the system is given in Figure 15.

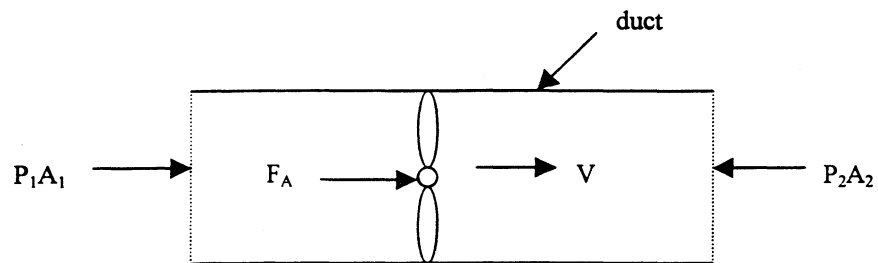


Figure 15. Ducted fan

m = mass flowrate ρ = density
 V = velocity Q = mass flowrate
 P = pressure F_A = anchoring force
 A = duct cross-sectional area

$$\dot{m}_1 = \dot{m}_2$$

$$\rho_1 = \rho_2$$

$$V_1 = V_2$$

$$A_1 = A_2 = A = \frac{\pi}{4}d^2 = \frac{\pi}{4}(4.375in.)^2$$

$$Q_1 = Q_2$$

$$\Delta P = 0.175in.H_2O$$

From conservation of linear momentum,

$$-\dot{m}_1V_1 + \dot{m}_2V_2 = F_A + P_1A - P_2A$$

$$\rightarrow F_A = A(P_2 - P_1) = A\Delta P$$

Convert ΔP from in H_2O to psi:

$$0.175in.H_2O \left(62.4 \frac{lb}{ft^3} \right) \left(\frac{1ft}{12in} \right)^3 = 0.006319psi$$

So the anchoring force required to maintain a ΔP of 0.175 in. of water with a fan of diameter 4.375 in. is

$$F_A = \frac{\pi}{4}(4.375)^2(0.006319) = 0.095lb.$$

5.2 Dynamic force calculation

The dynamic force is a varying axial force generated by interaction between the blades and a spatially non-uniform inflow. Acoustically, this interaction is seen as body forces acting on a fluid. The linearized equation of state, an inhomogeneous wave equation that describes the acoustic pressure generated by the body forces, is given by

$$\nabla^2 p - \frac{1}{c^2} \frac{\partial^2 p}{\partial t^2} = \nabla \cdot \vec{F}$$

$$\vec{F} = F_o \hat{e}_z \delta^3(\vec{r}) e^{i\omega t}, \quad \nabla \cdot \vec{F} = F_o \frac{\partial}{\partial z} (\delta^3(\vec{r})) e^{i\omega t},$$

where p is the acoustic pressure, c phase speed of the wave, t is time, F is the time-varying, harmonic body force per unit volume acting on the fluid, and F_o is the amplitude of the body force. This equation can be solved by considering the equation for a point source, which is given by

$$\nabla^2 p - \frac{1}{c^2} \frac{\partial^2 p}{\partial t^2} = -4\pi A \delta(\vec{r}) e^{i\omega t},$$

for which the solution is

$$p = \frac{A}{|\vec{r}|} \exp[i(\omega t - k|\vec{r}|)].$$

Multiply both sides of the body-force equation by $-4\pi A/(-4\pi A)$ and let

$$\phi = \frac{-4\pi A p}{\frac{\partial}{\partial z} F_o}.$$

Then the body-force equation is transformed into the point-source equation in terms of ϕ .

The resulting solution is given by

$$\begin{aligned} p &= \frac{\partial \phi}{\partial z} \frac{F_o}{-4\pi A} = \frac{-F_o}{4\pi} \frac{\partial}{\partial z} \left[\frac{1}{|\vec{r}|} \exp[i(\omega t - k|\vec{r}|)] \right] \\ &= \frac{F_o}{4\pi} \frac{1}{|\vec{r}|^2} \exp[i(\omega t - k|\vec{r}|)] (1 + k|\vec{r}|) \end{aligned}$$

Consider a body force producing acoustic radiation at the blade passage frequency (BPF).

The magnitude F_o of the dynamic force can be estimated by measuring the amplitude of acoustic radiation p_o from a fan at the BPF. Solving for F_o gives

$$F_o = \frac{4\pi r^2 p_o}{1 + kr}$$

So for an axial fan producing a SL of 40 dB at a BPF of 285 Hz and a distance of $r = 56$ in., the dynamic axial force can be calculated:

$$20 \log\left(\frac{p_o}{20 \mu Pa}\right) = 40 dB \rightarrow p_o = 0.29 \times 10^{-6} \text{ psi}$$

$$k = \frac{\omega}{c} = \frac{2\pi f}{c} = \frac{2\pi(285)}{343} \left(0.3048 \frac{m}{ft}\right) = 5.22 m^{-1} \left(0.3048 \frac{m}{ft}\right) = 1.59 ft^{-1} = 0.13 in^{-1}$$

$$F_o = \frac{4\pi(56)^2(0.29 \times 10^{-6})}{1 + (0.13)(56)} = 0.00138 lb = 0.022 oz.$$

Note that the dynamic force is only a small fraction of the static force. It is our intent to measure this dynamic force and correlate it with the SPL of the fan at the BPF.

5.3 Magnetic force in motor

In addition to the static and dynamic forces generated by the rotating fan blades, there is a force generated by something in the motor. Perhaps it is a magnetic force. The cause and magnitude of this force are unknown at this time. However, it is known that this force is greater than the static force because it always pulls the shaft and fan in toward the motor (flow direction makes fan want to move away from motor).

5.4 Measurement apparatus

An apparatus for measuring the static and dynamic axial forces in the shaft of the fan has undergone many design iterations.

5.4.1 Design 1 – strain gage

The original design consisted of a collar, fixed to the shaft, which pushed against a cantilever beam. A strain gage was attached to the cantilever so that the forces could be determined. The cantilever was attached to the frame, which supports the motor and positions the fan blades in a hole in a flat plate. A photograph of the apparatus is given in Figure 16.

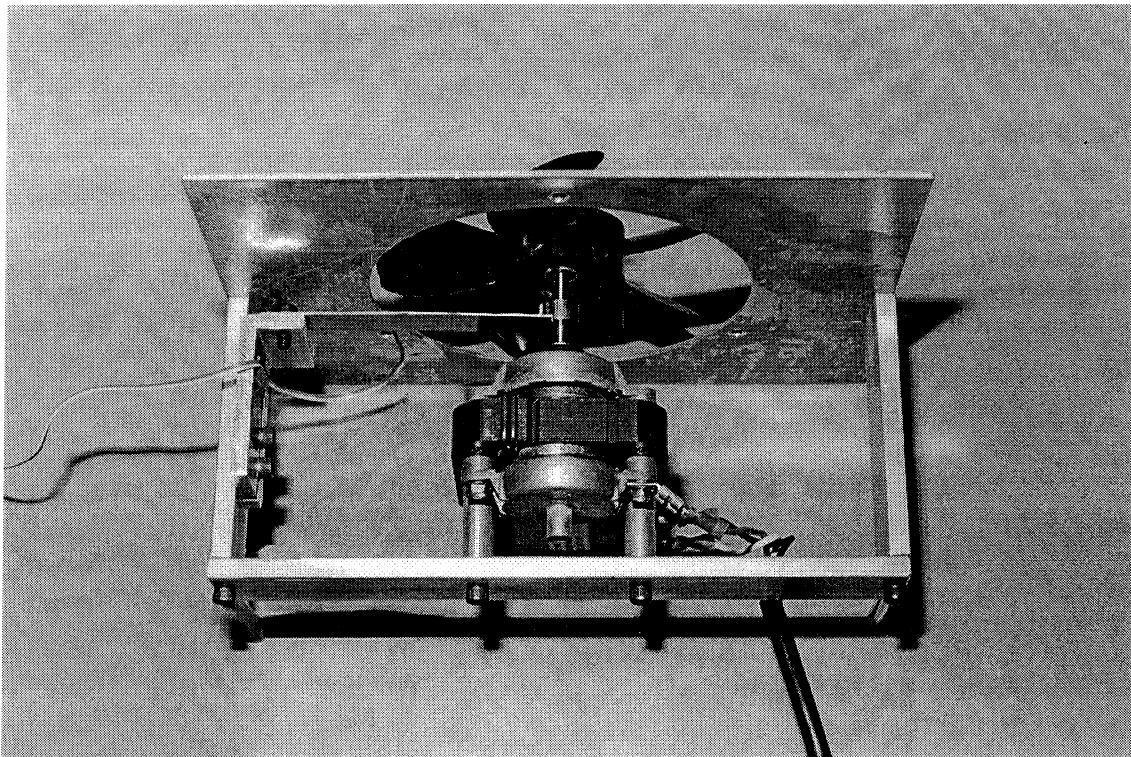


Figure 16. Original axial force measurement apparatus (photo by A.J. Paris)

The collar was made of brass for two reasons. The first reason is that brass can be machined to be very smooth. This way, unevenness in the surface, which would appear as axial forces in strain gage measurements, can be minimized. The second reason is that brass is somewhat naturally lubricated; the friction between the cantilever, also made of brass, and the collar should be minimized. A layer of oil or grease can be applied to further reduce the friction.

The strain gage used in the original design was a Micro-Measurements CEA-13-125UN-120 general-purpose gage with a resistance of 120 Ω and a gage factor of 2.110 (See Appendix for more information). A photograph of the gage, attached to the cantilever, is given in Figure 17.

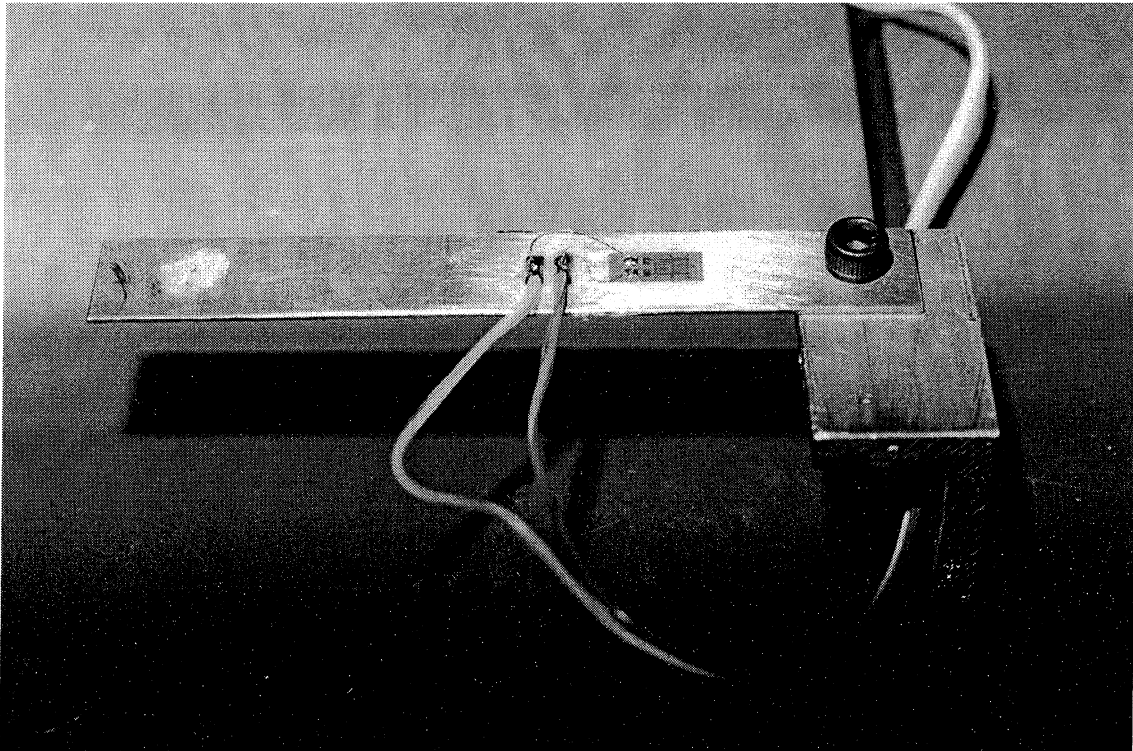


Figure 17. Strain gage on cantilever (photo by A.J. Paris)

The FFT of the strain gage signal contained peaks at the fan revolution frequency and at the BPF, but a peak at $2*BPF$ could not be distinguished above the noise level. These results are shown in Figure 18.

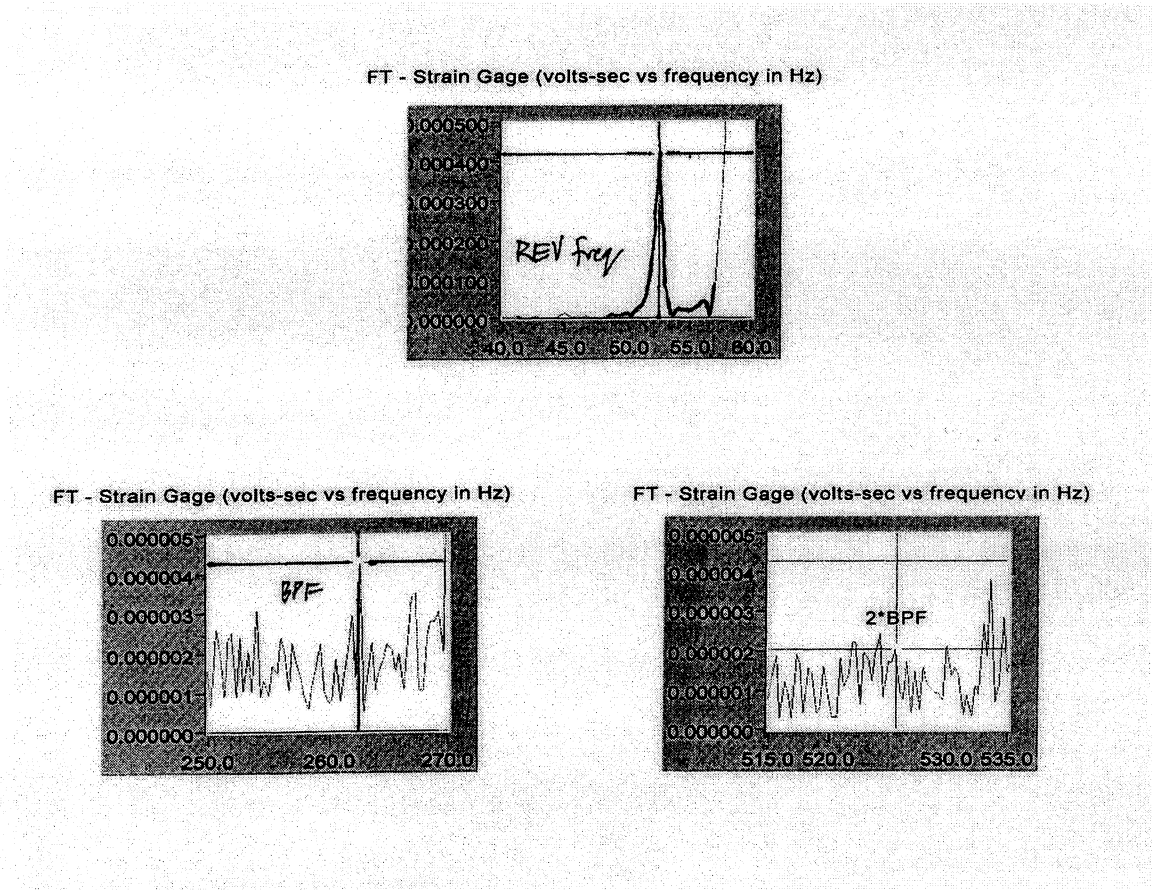


Figure 18. Design 1 – Results

In order to make sure that the peak at the BPF was really the dynamic axial force generated acoustically, a theoretical prediction of the strain was made. The SL of a 6 Hz

band centered at the BPF (264 Hz) is 42.82 dB at a distance of 3 ft. This SL is converted to acoustic pressure by the relation

$$SL = 20 \log \left(\frac{P_o}{P_{ref}} \right), \quad P_{ref} = 20 \mu Pa$$

$$\Rightarrow P_o = 0.00277 Pa \left(\frac{14.5 psi}{1 \times 10^5 Pa} \right) = 0.401 \times 10^{-6} psi$$

Using the acoustic pressure, the magnitude of the force F_o from the air on the blade can be calculated:

$$F_o = \frac{P_o 4\pi r^2}{1 + kr}$$

where

$$k = \frac{\omega}{c} = \frac{2\pi f}{c}$$

is the wave number. Then,

$$F_o = \frac{P_o 4\pi r^2}{1 + \frac{2\pi f}{c} r} = \frac{(0.401 \times 10^{-6} psi)(4\pi)(36in)^2}{1 + \frac{2\pi(264s^{-1})}{343m/s} (0.3048 \frac{m}{ft}) (\frac{1ft}{12in})(36in)} = 0.00123lb$$

$$F_o = 0.00123lb \times 4.448 \frac{N}{lb} = 0.0055N.$$

By modeling the fan and shaft as a rigid body and the cantilever beam as a linear spring, the maximum displacement generated by F_o can be estimated. The equation of motion for the mass-spring system is given by

$$m\ddot{x} + kx = \underline{F_o} e^{i\omega t},$$

where m is the mass of the fan plus the shaft, and k is the experimentally-determined stiffness of the cantilever (see Appendix). Using complex analysis, the magnitude of the displacement of the tip of the cantilever is given by

$$|x|_{\max} = \frac{|F_o|}{k - m\omega^2} = \frac{|F_o|}{k} \frac{1}{\left|1 - \left(\frac{\omega}{\omega_n}\right)^2\right|},$$

where $\omega_n^2 = k/m$ is the natural frequency of the system. So,

$$\omega_n = \sqrt{\frac{184 \text{ N/m}}{0.1 \text{ kg}}} = 43 \frac{\text{Rad}}{\text{s}}$$

$$|x_p|_{\max} = \frac{0.0055 \text{ N}}{184 \text{ N/m}} \frac{1}{\left|1 - \frac{2\pi 164 \text{ s}^{-1}}{43 \text{ Rad/s}}\right|} = 20 \text{ nm}.$$

It is apparent from the dominance of the second term in the above denominator that the result is almost independent of k , the cantilever stiffness, at least for small k . Thus it is the mass that limits the displacement (mass-controlled).

Knowing the displacement of the tip of the cantilever, the strain induced at the location of the strain gage can then be determined. A diagram of the cantilever is given in Figure 19.

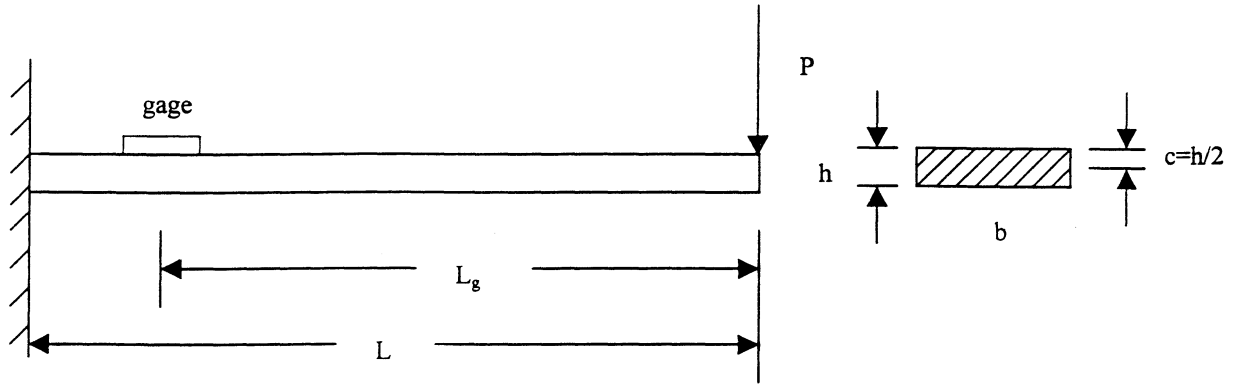


Figure 19. Cantilever with strain gage

From mechanics of materials, the strain at the gage location is given by

$$\varepsilon_g = \frac{M_g c}{EI} = \frac{PL_g c}{EI},$$

but the deflection $\delta = |x_p|_{\max}$ of the tip of the cantilever is given by

$$\delta = \frac{PL^3}{3EI} \Rightarrow P = \frac{3EI\delta}{L^3}$$

$$\Rightarrow \varepsilon_g = \frac{3\delta L_g c}{L^3} = \frac{3(20nm)(60.2mm)(\frac{0.8204}{2}mm)}{(74.27mm)^3} = 3.6n\varepsilon$$

Since the strain gage cannot detect strains below $1 \mu\varepsilon$, another method must be used to determine axial force.

5.4.2 Design 2 – accelerometer

In the second design, the strain gage was replaced by an accelerometer, which was attached to the cantilever near the tip. A photograph of design 2 is given in Figure 20.

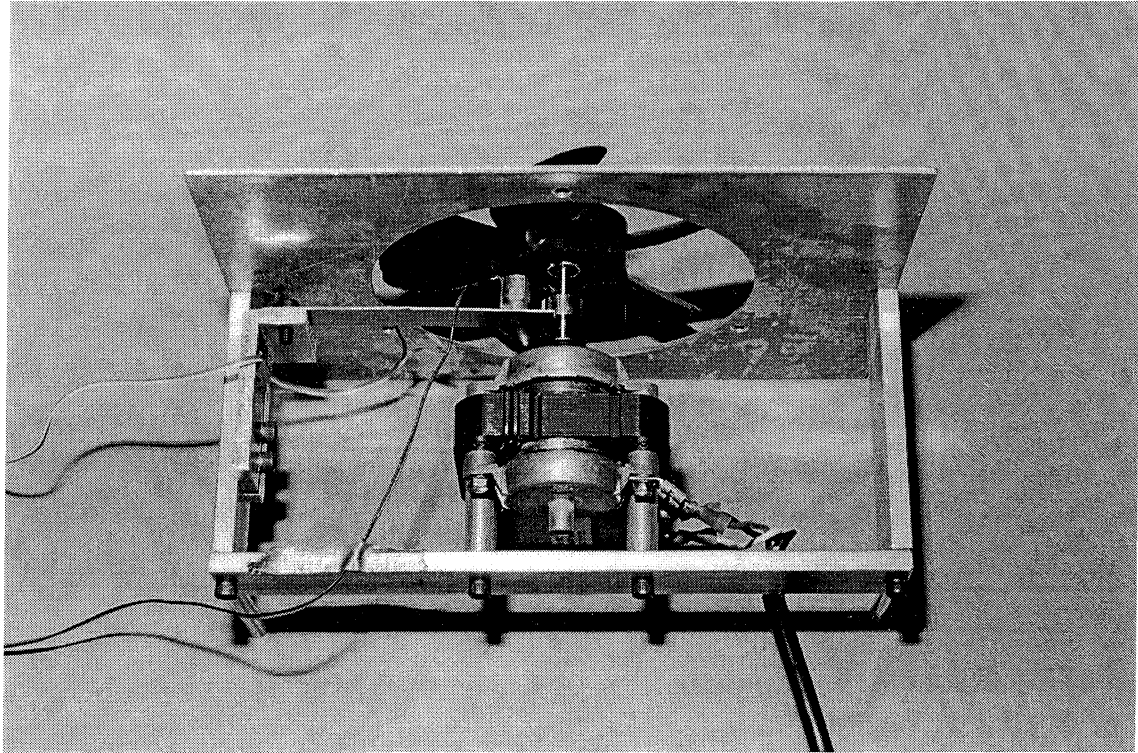


Figure 20. Design 2 – accelerometer (photo by A.J. Paris)

The FFT of the accelerometer signal contained sharp peaks at the BPF and also at its harmonics. However, the FFT also contained peaks similar, and in some cases larger, in magnitude at *all* multiples of the revolution frequency. The measurement was performed with the blades removed (in order to see if these responses were acoustic), but the peaks at all multiples of the revolution frequency were still there. These results are shown in Figures 21 and 22.

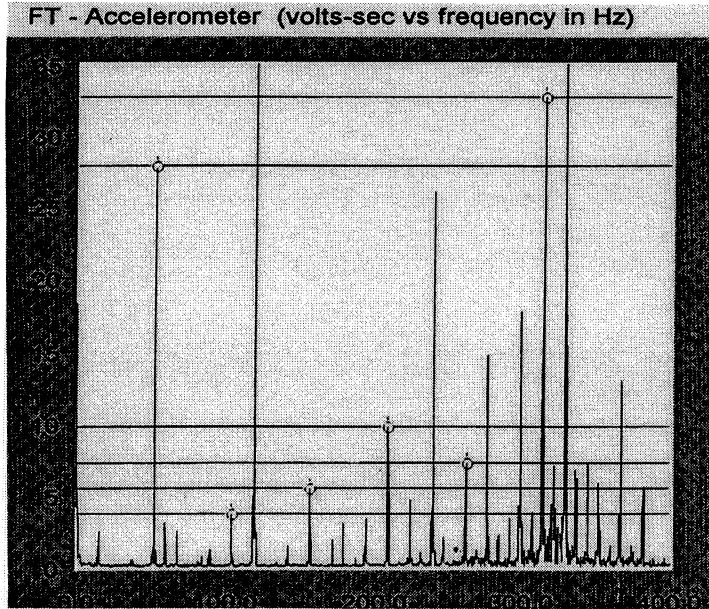


Figure 21. Design 2 – Results: With blades

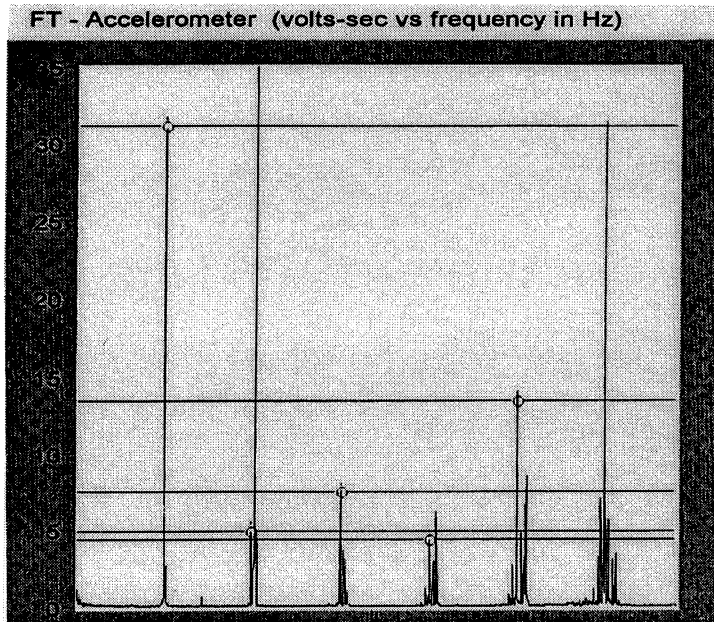


Figure 22. Design 2 – Results: Without blades

This result indicates that there is another source of axial force motion. To compare the observed peak at the BPF with the expected peak generated acoustically, a calculation was made to predict the magnitude of the FFT at the BPF. The rms voltage contained in a given frequency band is given by

$$(V_{rms})^2 = \frac{2}{N} \sum_{band} |FFT|^2,$$

where N is the number of total samples. The voltage is related to the acceleration a via the accelerometer calibration constant. So, for a band of 1 Hz, the magnitude of the FFT is given by

$$|FFT| = \left(\frac{N^2}{2} V_{rms}^2 \right)^{1/2} = \frac{N}{2} \frac{a}{3446 \frac{m/s^2}{volt}}.$$

The magnitude of the acceleration of the tip of the cantilever is determined from the maximum displacement:

$$|a|_{max} = \omega^2 |x|_{max} = (2\pi 164s^{-1})^2 (20nm) = 0.055 \frac{m}{s^2}.$$

So the predicted magnitude of the FFT is

$$|FFT| = \frac{24000samples}{2} \frac{0.055 m/s^2}{3446 \frac{m/s^2}{volt}} = 0.19volts.$$

This peak is much less than the peak that is actually present at the BPF and at other multiples of the revolution frequency as well. This result further confirms the notion that something else in the system is generating axial movement.

5.4.3 Design 3 – pulleys

It is believed that the unwanted source of axial motion at multiples of the revolution frequency is coming from the motor (dynamic magnetic motor forces). In order to eliminate this motion, a pulley system was implemented into the design. By driving the fan with pulleys, the motor speed and fan speed are different. Hence, the BPF and harmonics thereof will be different from the motor revolution speed's harmonics (the frequencies at which motor axial forces occur). In addition, axial motion from motor forces will not be easily transmitted through the pulley belt. A photograph of Design 3 is given in Figure 23. Note that the new design can accommodate a larger, and hence more sensitive, accelerometer.

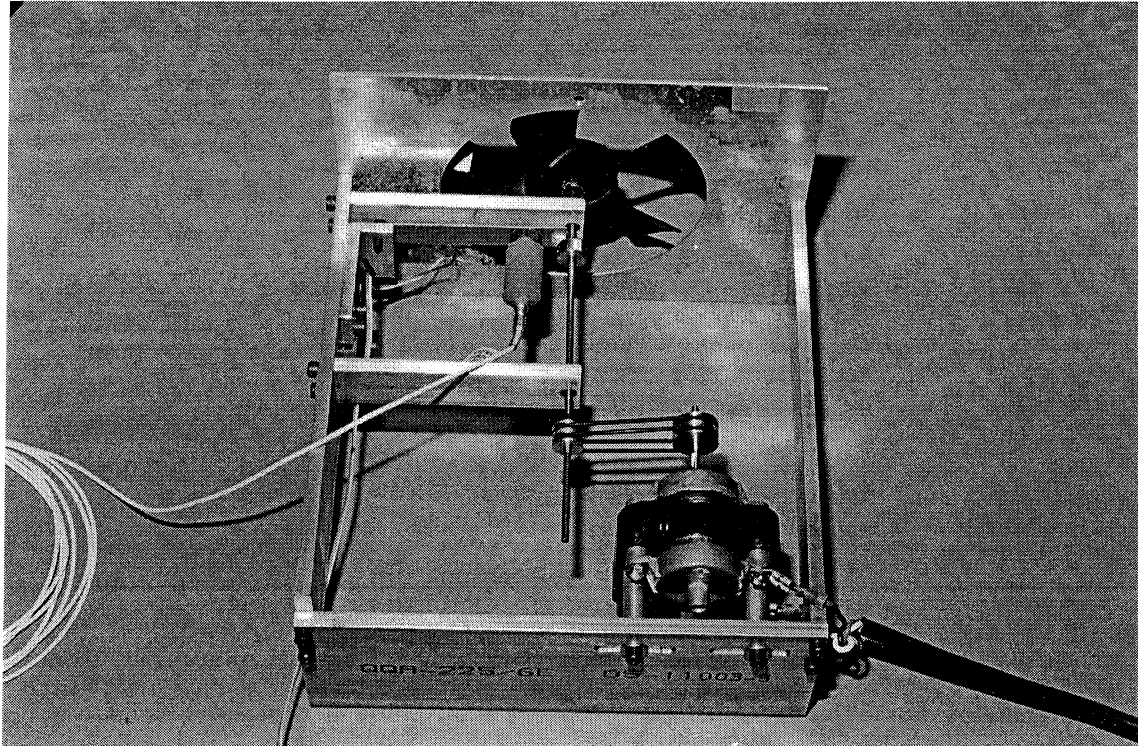


Figure 23. Design 3 – pulleys (photo by A.J. Paris)

Unfortunately, the FFT of the accelerometer signal still contains peaks at the revolution frequency and harmonics. In addition, the pulley system decreased the motor speed from 59 Hz (no pulley connection) to 21 Hz (pulley connection). The speed of the fan is about 33 Hz, depending on the tension in the belts. When the fan is removed from the shaft (but the pulleys are still connected), the motor almost achieves its normal operating speed of around 59 Hz. The results from Design 3 are given in Figure 24.

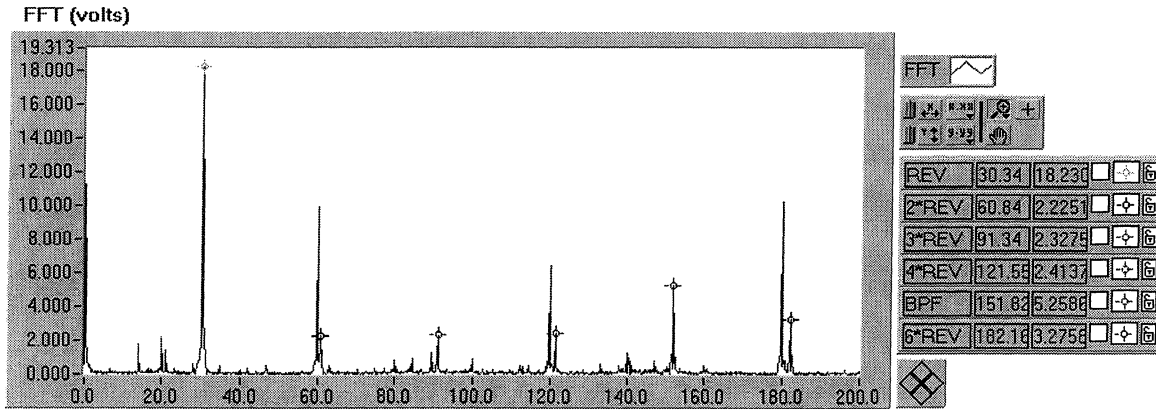


Figure 24. Design 3 – Results

As previously calculated, the magnitude of the displacement of the cantilever is estimated to be about 20 nm. However, since the fan speed has been nearly cut in half, the displacements in Design 3 should be reduced as well. In any event, the roughness of the collar is greater than 20 nm and is thus thought to be the source of axial motion.

5.4.4 Design 4 – silicon / Teflon

In order to decrease the axial motion generated by the roughness of the collar, a single crystal silicon washer was made and then epoxied to the collar. A piece of Teflon was epoxied to the cantilever to further enhance the smoothness of the contact. A photograph of Design 4 is given in Figure 25.

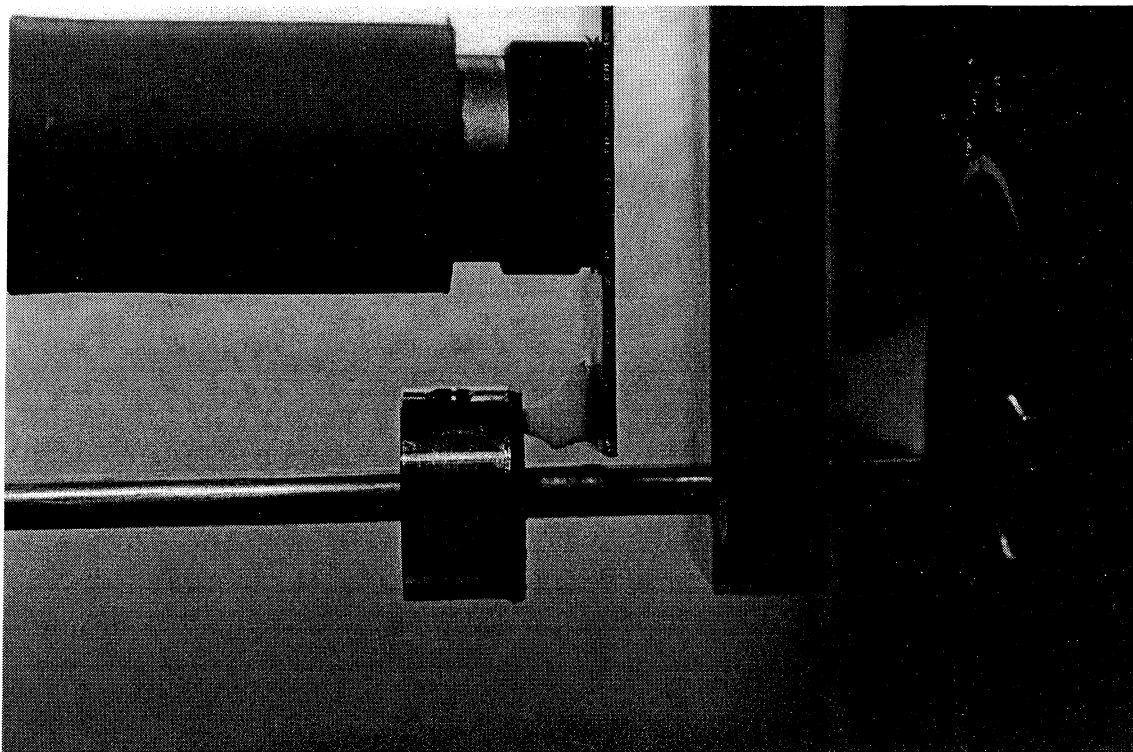


Figure 25. Design 4 – silicon / Teflon (photo by A.J. Paris)

The roughness of the silicon washer was measured using the Dektak³ ST Surface Profiler at the Center for Microanalysis of Materials in the Materials Research Laboratory at UIUC (Ferney, 1999). The roughness was approximately 50 nm (see Appendix).

Although the roughness is greater than the predicted cantilever tip displacements, it is much smoother than the collar. Hence, if roughness is indeed the source of axial motion, an improvement should be seen in the results. The results for Design 4 are given in Figure 26.

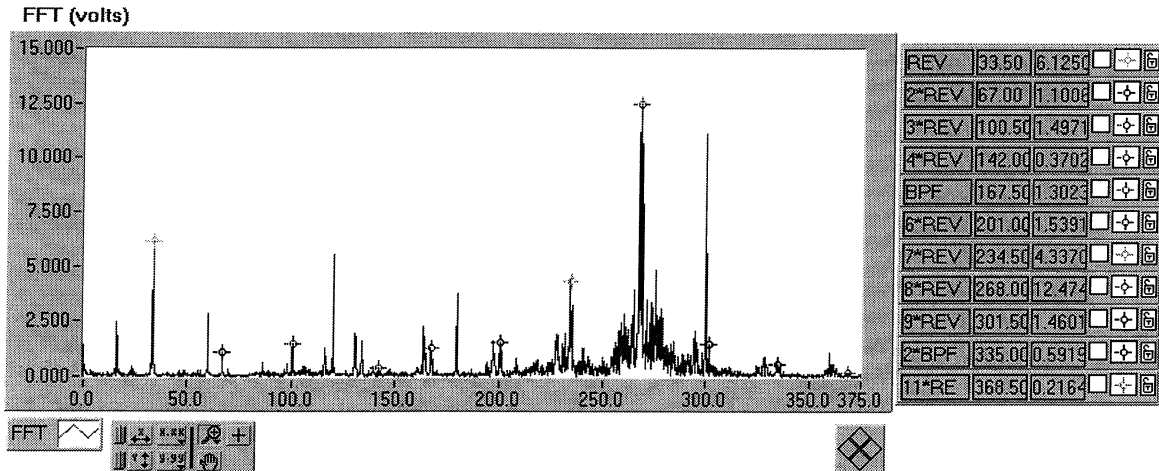


Figure 26. Design 4 – Results

These results are better than previous ones, but there is still some axial motion. The peak at the BPF corresponds to a cantilever tip displacement of about 41nm, which is still significantly greater than what we expect to see (<20nm). Also, the silicon/Teflon contact did not behave as expected. The Teflon flaked off onto the silicon, and the contact generated a loud squeaking sound.

5.5 Conclusions

A method for measuring the dynamic axial force generated by a steady, non-uniform flow field is investigated. Experimental results show that using a cantilevered system to measure the axial shaft displacements generated by the blade-flow interaction may not be the best approach since the measurement system introduces additional sources of axial motion, which occur at the frequencies of interest. If it is possible to eliminate, or significantly reduce, all other sources of axial motion, then the cantilever measurement system could be feasible as long as a sensitive enough accelerometer is used. A system

of strain gages is probably not sensitive enough to detect the tiny displacements of interest.

5.6 Recommendations for future work

Using the current apparatus, it might be possible to obtain better results by using an even smoother surface. The silicone wafer was significantly flawed, and it is possible to obtain one with a smoother surface roughness. Also, the shaft supports may be a source of axial force generation. Currently they are simply brass bushings. Perhaps using more sophisticated supports would help reduce unwanted axial force generation.

Another approach is to return to the original fan configuration, shaft directly coupled to motor. A different kind of motor that does not generate axial motion at its revolution speed and harmonics could be used. Perhaps then the cantilever system would work since the need for additional shaft supports would be eliminated. If there is still too much unwanted axial motion in the cantilever system, it could be eliminated completely, and a laser vibrometer could be used.

Once an axial force measurement device is developed, the correlation between dynamic axial force and acoustic radiation at the BFP can be studied by placing various upstream obstructions in the flow in order to generate different spatially non-uniform flow fields.


REFERENCES

- ACRC, 1999. Web page, <http://acrc.me.uiuc.edu>.
- American National Standard, ANSI S12.35-1990. "Precision methods for the determination of sound power levels of noise sources in anechoic and hemi-anechoic rooms", Accredited Standards Committee S12, Noise.
- Beranek, Leo. *Acoustics*, p362.
- Chiu, Wen-Shyang, G.C. Lauchle, and D.E. Thompson. February 1989. "Subsonic axial flow fan noise and unsteady rotor force", *J. Acoust. Soc. Am.* 85 (2).
- Curle, N. 1955. "The influence of solid boundaries upon aerodynamic sound", *Proc. Royal Soc. London.* A 231, 505-514.
- Foley, D. W., instrument maker, University of Illinois at Urbana-Champaign. 1999. Personal communication.
- Ferney, B., graduate student in Theoretical and Applied Mechanics, University of Illinois at Urbana-Champaign. 1999. Personal communication.
- International Standard, ISO 3745-1977. "Acoustics – Determination of sound power levels of noise sources – Precision methods for anechoic and semi-anechoic rooms", first edition – 1977-05-15.
- Kinsler, Frey *et al.* 1982. *Fundamentals of Acoustics*, 3rd ed.
- Lauchle, G.C., J.R. MacGillivray and D.C. Swanson. January 1997. "Active control of axial-flow fan noise", *J. Acoust. Soc. Am.* 101 (1).
- Lighthill, M.J. 1952. "On sound generated aerodynamically. I. General theory", *Proc. Royal Soc. London.* A 211, 564-587.
- National Instruments Corporation, 1996. *LabVIEW Help*.

- Neise, W. 1992. "Review of fan noise generation mechanisms and control methods",
Proceedings from Fan Noise, An International INCE Symposium. 45-56.
- Paris, A.J., Visiting Assistant Professor of Theoretical and Applied Mechanics,
University of Illinois at Urbana-Champaign. 1999. Personal communication.
- Peterson, A. and E. Gross Jr. *Handbook of Noise Measurement*, 7th ed.
- Quinlan, D.A. November-December 1992. "Application of active control to axial flow
fans", *Noise Control Engineering Journal* 39 (3).
- Schomer, P., Professor of Mechanical Engineering, University of Illinois at Urbana-
Champaign. 1999. Personal communication.
- Washburn, Karl B. and G.C. Lauchle. September-October 1988. *Noise Control
Engineering Journal* 31 (2).

APPENDIX

A1. Strain gage

 <p>Micro-Measurements Division <i>Made In USA</i></p> <p>MEASUREMENTS GROUP, INC. RALEIGH, NORTH CAROLINA</p> <div style="border: 2px solid black; padding: 5px; text-align: center; font-weight: bold; font-size: 1.2em;"> PRECISION STRAIN GAGES </div>	OPTION CODE 983611	LOT NUMBER R-A48AF42	QUANTITY 5 GAGES	GAGE TYPE 120.0 ±0.3%	RESISTANCE IN OHMS AT 24°C 2.110 ±0.5%	GAGE FACTOR AT 24°C (+0.8 ±0.2)%	CEA-13-125UN-120 CEA-13-125UN-120
---	---------------------------------	--------------------------------	----------------------------	---------------------------------	--	--	--------------------------------------

GENERAL INFORMATION: CEA-SERIES STRAIN GAGES

GENERAL DESCRIPTION: CEA gages are a general-purpose family of constant strain gages widely used in experimental stress analysis. The gages are supplied with a fully encapsulated grid and exposed copper-coated integral solder tabs.

TEMPERATURE RANGE: -100° to +400° F (-75° to +205° C) for continuous use in static measurements.

SELF-TEMPERATURE COMPENSATION: See data curve below.

STRAIN LIMITS: Approximately 5% for gage lengths 1/8 in (3.2 mm) and larger; and approximately 3% for gage lengths under 1/8 in (3.2 mm).

FATIGUE LIFE: Fatigue life is a marked function of solder joint formation. With 30-AWG leads directly attached to gage tabs, fatigue life will be 10⁶ cycles at ±1500 μin/in (μm/m) using *M-Line* 361A solder.

CEMENTS: Compatible with M-M Certified M-Bond 200, but it will normally not provide the greatest strain limit. Micro-Measurements M-Bond AE-10/15, M-Bond GA-2, M-Bond 600, and M-Bond 610 are excellent. M-Bond 610 is the best choice over the entire operating range. Refer to M-M Catalog A-110 for information on bonding agents, and Bulletins B-127, B-130, and B-137 for installation procedures.

SOLDER: If operating temperature will not exceed +300° F (+150° C), *M-Line* solder 361A (63-37) tin-lead solder may be used for lead attachment. *M-Line* solder 450 (95-5) tin-antimony is satisfactory to +400° F (+205° C). Refer to M-M Catalog A-110 for further information on solders, and Tech Tip TT-609 for lead attachment techniques.

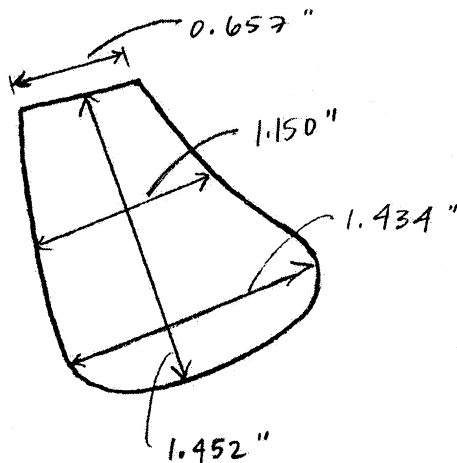
BACKING: The backing of CEA-Series gages has been specially treated for optimum bond formation with all appropriate strain gage adhesives. No further cleaning is necessary if contamination of the prepared surface is avoided during handling.

G045 FORM: 962516CJD

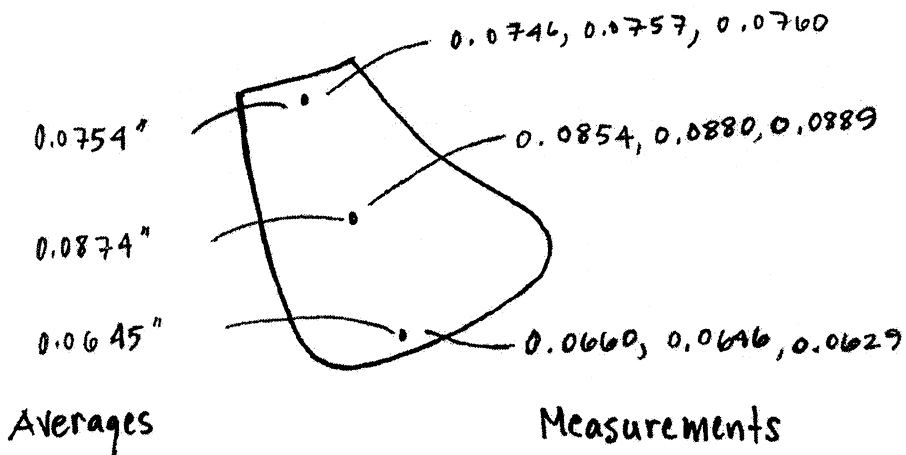
A2. Fan properties

The fan used in this work is a 5-bladed, 4.375" diameter, plastic refrigerator compressor fan. Blade dimensions, weight, and stiffness are given below. (blade stiffness graphs made by A.J. Paris)

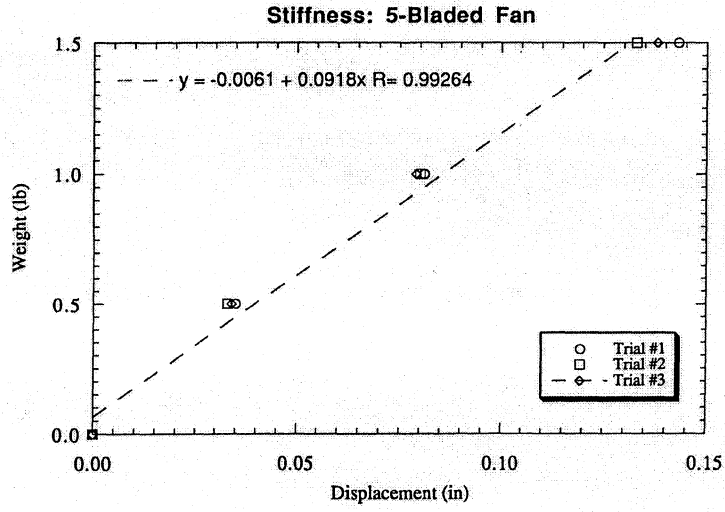
5-Bladed Fan



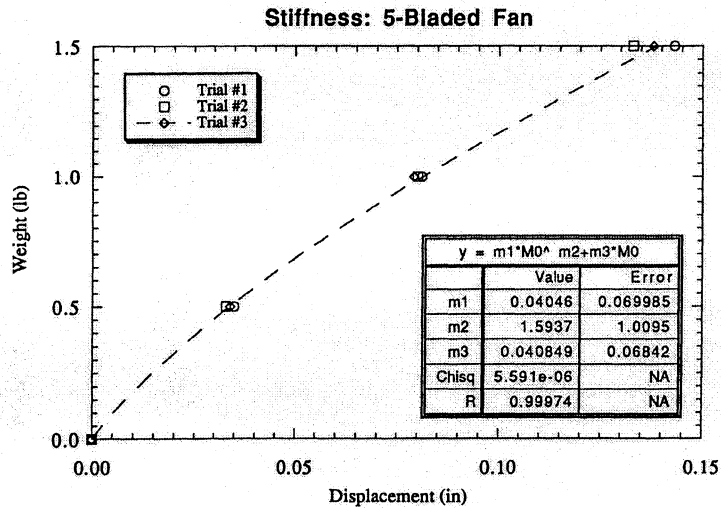
Fan Dia. = 4.375"
Hub Dia. = 1.550"
Blade Wt. = 0.0036 lb
= 1.6 g



Thicknesses



$$k = 10.89 \text{ lb/in}$$



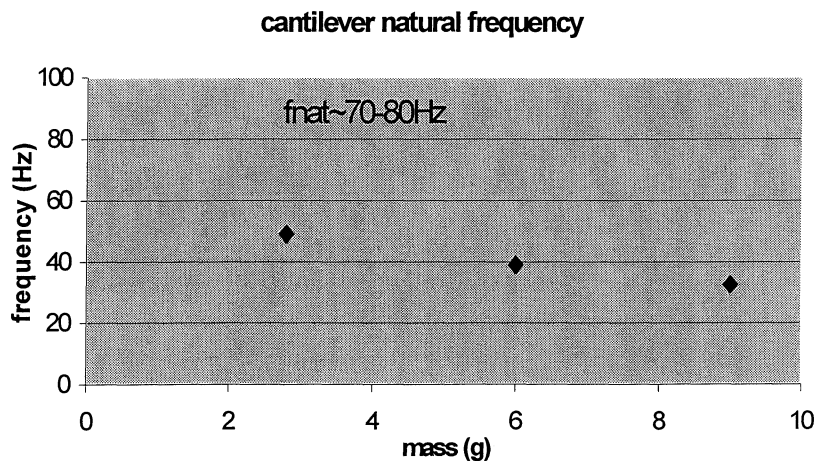
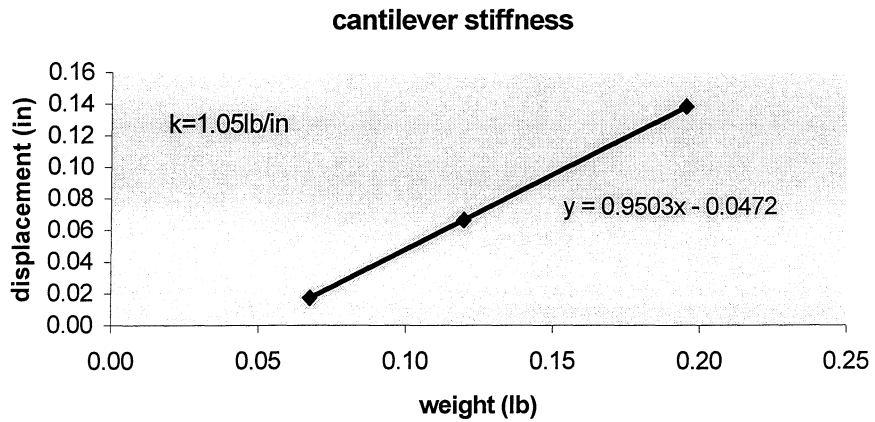
$$k|_{\text{Disp}=0} = 24.48 \text{ lb/in}$$

A3. Cantilever properties

The measured dimensions, stiffness, and natural frequency of the brass cantilever used for axial force measurement are given below.

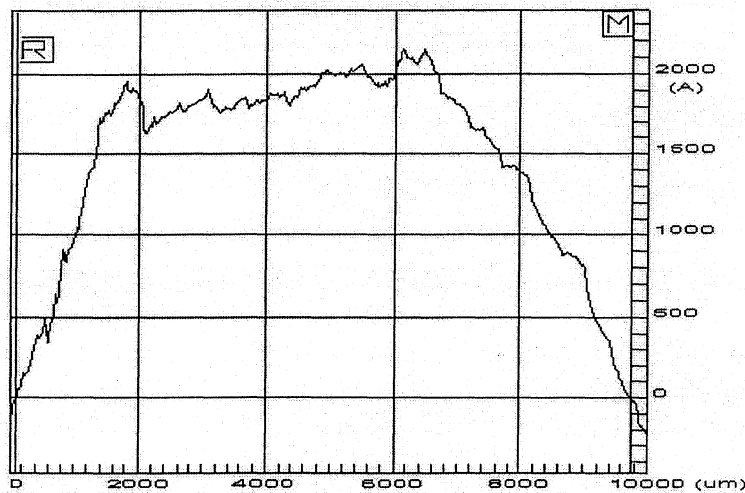
cantilever dimensions		
thickness (h) :	0.0323 in	0.8204 mm
height (b) :	0.4984 in	12.66 mm
length (L) :	2.924 in	74.27 mm
length to mid-gage (L_{gage}) :	2.37 in	60.2 mm

material properties		
material :	yellow brass	
modulus :	15×10^6 psi	105 GPa
specific weight :	0.306 lb / in ³	
density :		8470 kg / m ³



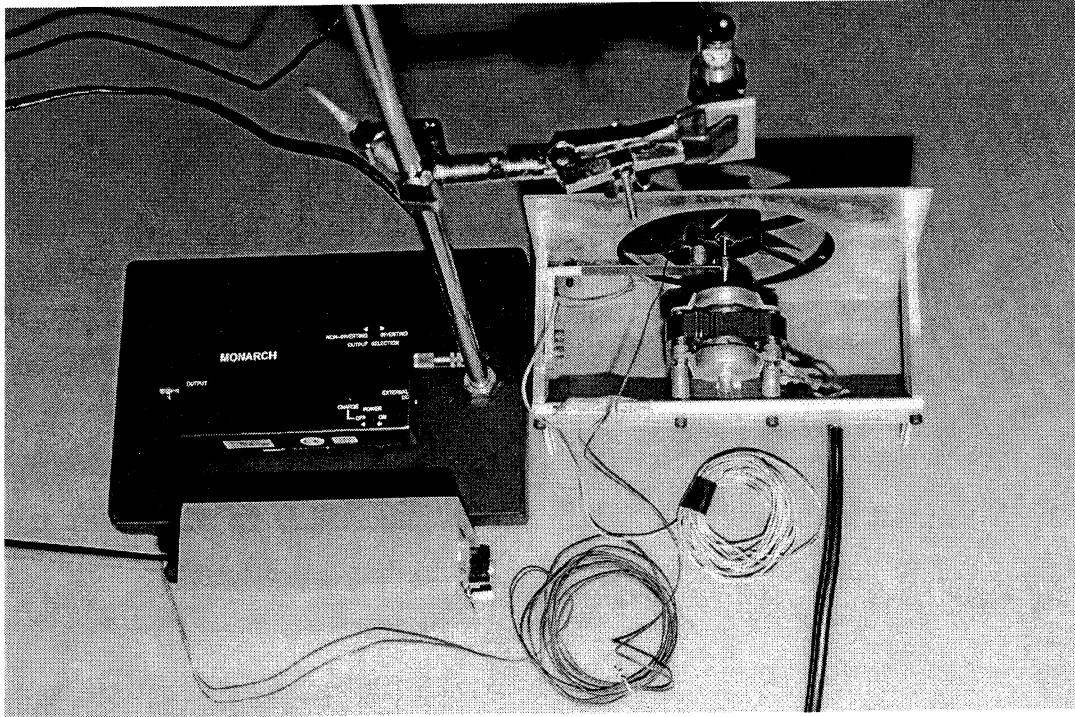
A4. Silicon roughness

The surface roughness of the single crystal silicon washer used for axial force measurements was determined at the Center for Microanalysis of Materials in the Materials Research Laboratory at UIUC using a Dektak³ Surface Profiler with the help of Brook Ferney, TAM Dept. The results are given below.

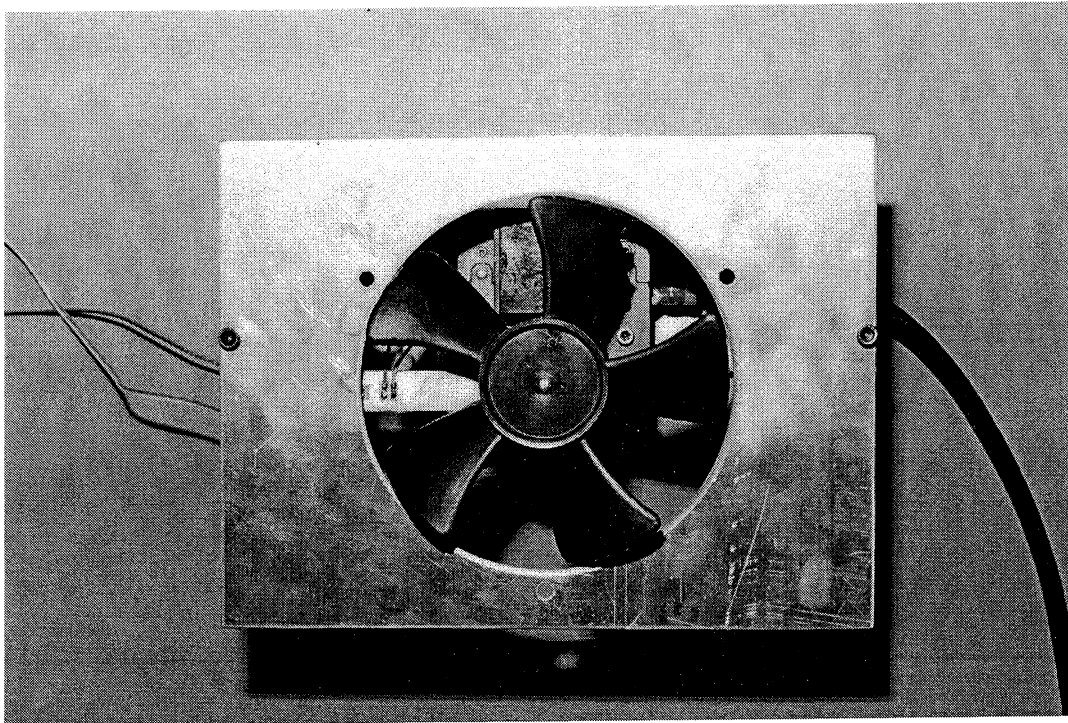


```
DEKTAK 3ST Version 2.12
PROG FILE NAME: omm.mp
SCAN ROUTINE #: 20
TIME OF SCAN: 14:35:47 Thu Oct 28 1999
DATA FILE NAME: .020
Scan ID..... 0
Scan Length..... 10000um
Scan Speed..... Low (50 sec)
Data Res..... Medium
Data Points..... 4000
Resolution..... 2.500 um/sample
Meas. Range..... 655 KA
Profile..... Hills&Valleys
Stylus Force..... 15mg
Soft Touch..... No
Ramp-Up Mode..... Off
R. Cursor..... 0A @ 100.00um
M. Cursor..... 5A @ 9755.43um
Vert. Delta..... 5A
Horiz. Delta... 9655.43um
ANALYTIC FUNCTIONS:
Rax = 477.355A           R:um; M:um
Avg_ht = 1490.286A     100.00  9755.43
                       100.00  9755.43
```

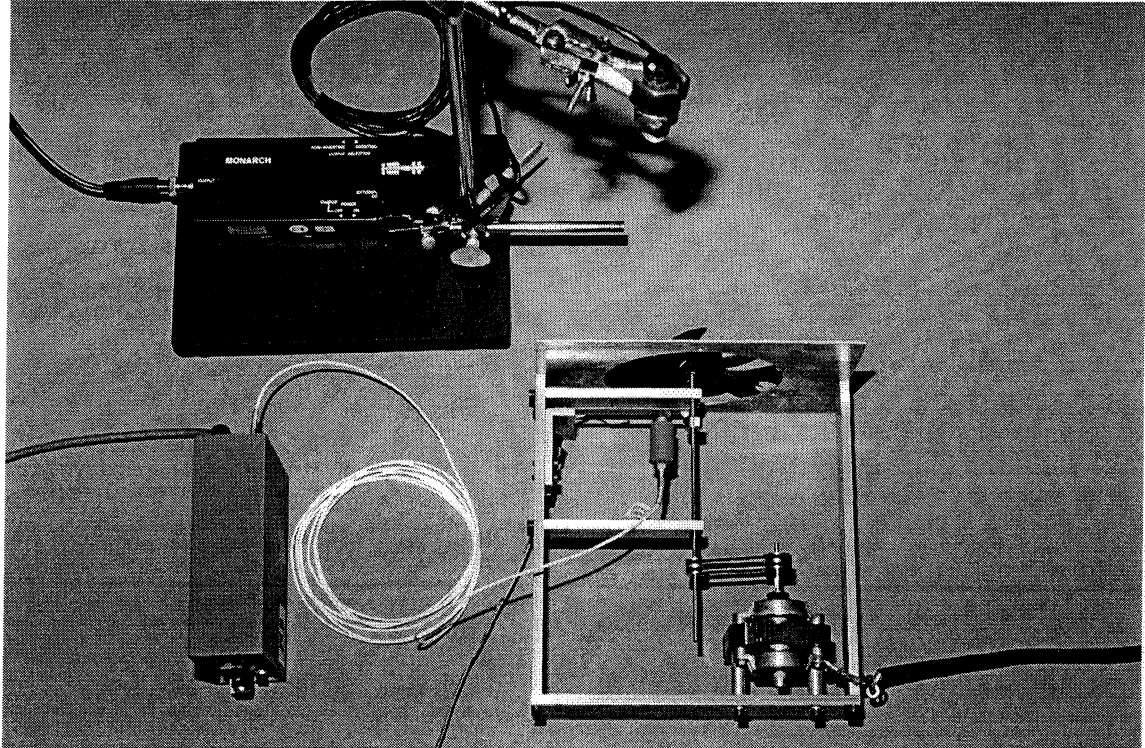
A5. Photographs



Setup: Designs 1&2 (photo by A.J. Paris)



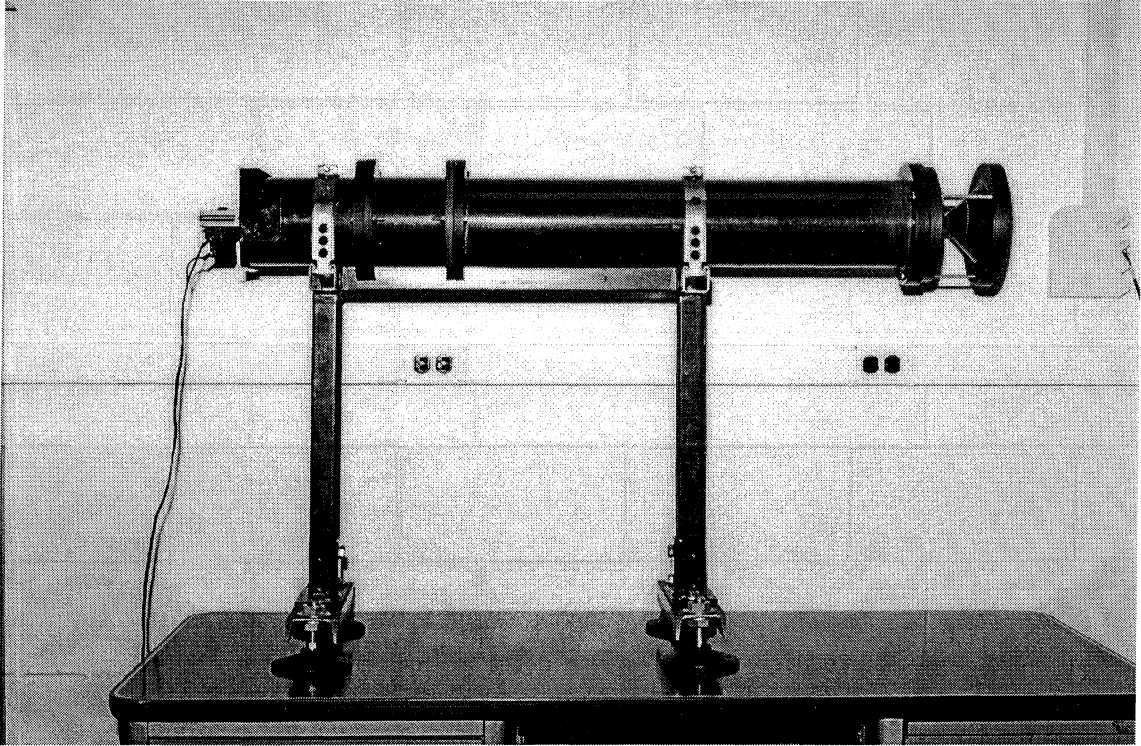
Front view (photo by A.J. Paris)



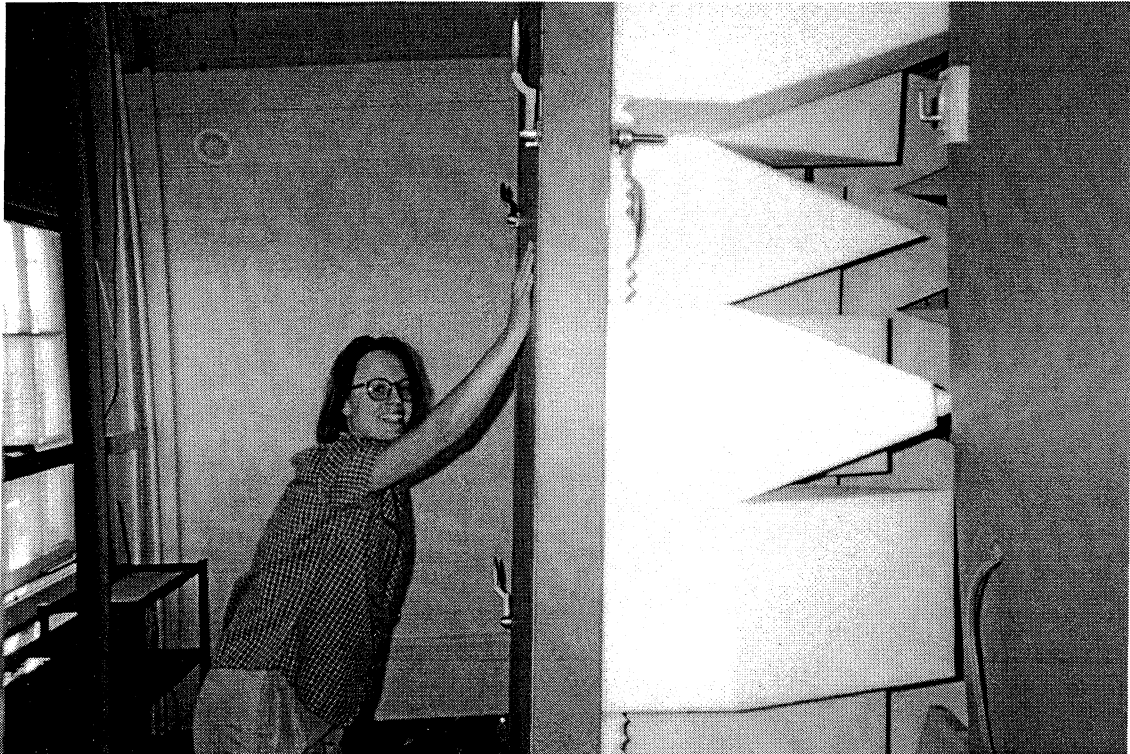
Setup: Designs 3&4 (photo by A.J. Paris)



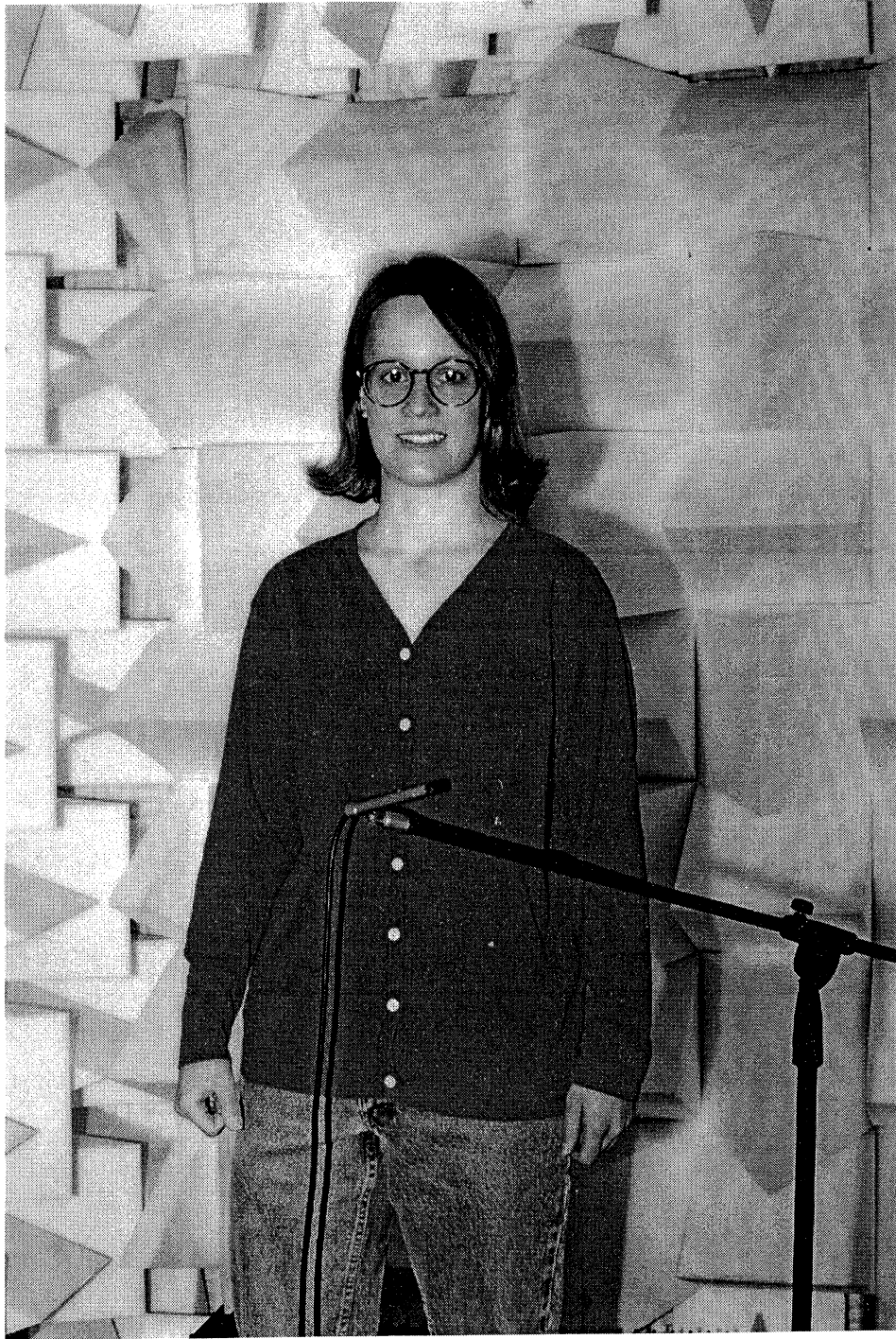
Sarah Zeller in lab, 355 MEL (photo by A.J. Paris)



Duct test section (photo by A.J. Paris)



Anechoic chamber door (photo by K.E. Zeller)



Inside anechoic chamber, with microphone (photo by A.J. Paris)

List of Tables

Table 1. Path #1 Deviations	17
Table 2. Path #2 Deviations	18
Table 3. Path #3 Deviations	18
Table 4. Path #4 Deviations	18

List of Figures

Figure 1. Fan noise generation mechanisms (Neise, 1992)	5
Figure 2. Anechoic chamber	14
Figure 3. Qualification: Path #1 – On axis	16
Figure 4. Qualification: Path #2	16
Figure 5. Qualification: Path #3	16
Figure 6. Qualification: Path #4 – straight up	17
Figure 7. Setup	20
Figure 8. Acoustic frequency response of 5-bladed fan	22
Figure 9. Theoretical dipole beam pattern	22
Figure 10. Directivity, SPL(dB) of fan at BPF and harmonics, $r = 52''$ (4-point averaging using 4-pt avg.vi)	23
Figure 11. Directivity, SPL(dB) of fan at BPF and harmonics, $r = 38.75''$ (avg. FFT of 10 synchronized acquisitions using AvgFFT.vi) (48,000 samples – 16,000 sa/sec)	24

Figure 12. Directivity, SPL(dB) of fan at BPF and harmonics, $r = 38.75''$ (avg. SL of 10 synchronized acquisitions using SyncBPFAvgdB.vi) (48,000 samples – 16,000 sa/sec)	24
Figure 13. Duct test section	25
Figure 14. Setup (G.C. Lauchle, J.R. MacGillivray, D.C. Swanson)	29
Figure 15. Ducted fan	37
Figure 16. Original axial force measurement apparatus	41
Figure 17. Strain gage on cantilever	42
Figure 18. Design 1 – Results	43
Figure 19. Cantilever with strain gage	46
Figure 20. Design 2 – accelerometer	47
Figure 21. Design 2 – Results: With blades	48
Figure 22. Design 2 – Results: Without blades	48
Figure 23. Design 3 – pulleys	51
Figure 24. Design 3 – Results	52
Figure 25. Design 4 – silicon / Teflon	53
Figure 26. Design 4 – Results	54